

The Evolution of X-ray Clusters of Galaxies

Piero Rosati^{1,3}, Stefano Borgani² and Colin Norman^{3,4}

¹ ESO – European Southern Observatory, D-85748 Garching bei München, Germany;
e-mail: prosati@eso.org

² Dipartimento di Astronomia dell’Università di Trieste, via Tiepolo 11, I-34131 Trieste, Italy;
e-mail: borgani@ts.astro.it

³ Department of Physics and Astronomy, The Johns Hopkins University, Baltimore, MD
21218, USA; e-mail: norman@stsci.edu

⁴ Space Telescope Science Institute, Baltimore, MD 21218, USA

KEYWORDS: cosmology, intracluster medium, temperature, masses, dark matter

ABSTRACT: Considerable progress has been made over the last decade in the study of the evolutionary trends of the population of galaxy clusters in the Universe. In this review we focus on observations in the X-ray band. X-ray surveys with the *ROSAT* satellite, supplemented by follow-up studies with *ASCA* and *Beppo-SAX*, have allowed an assessment of the evolution of the space density of clusters out to $z \approx 1$, and the evolution of the physical properties of the intra-cluster medium out to $z \approx 0.5$. With the advent of *Chandra* and *Newton-XMM*, and their unprecedented sensitivity and angular resolution, these studies have been extended beyond redshift unity and have revealed the complexity of the thermodynamical structure of clusters. The properties of the intra-cluster gas are significantly affected by non-gravitational processes including star formation and Active Galactic Nucleus (AGN) activity. Convincing evidence has emerged for modest evolution of both the bulk of the X-ray cluster population and their thermodynamical properties since redshift unity. Such an observational scenario is consistent with hierarchical models of structure formation in a flat low density universe with $\Omega_m \simeq 0.3$ and $\sigma_8 \simeq 0.7 - 0.8$ for the normalization of the power spectrum. Basic methodologies for construction of X-ray-selected cluster samples are reviewed and implications of cluster evolution for cosmological models are discussed.

CONTENTS

INTRODUCTION	2
PHYSICAL PROPERTIES OF GALAXY CLUSTERS	3
<i>X-ray properties of clusters</i>	5
<i>Cooling in the Intra Cluster Medium</i>	8
OBSERVATIONAL FRAMEWORK	9
<i>Optically-based Cluster Surveys</i>	9
<i>X-ray Cluster Surveys</i>	11
<i>Strategies and Selection Functions for X-ray Surveys</i>	14
<i>Other methods</i>	17
THE SPACE DENSITY OF X-RAY CLUSTERS	17
<i>Local Cluster Number Density</i>	17
<i>The Cluster Abundance at Higher Redshifts and Its Evolution</i>	18
<i>Distant X-ray Clusters: the Latest View from Chandra</i>	20

COSMOLOGY WITH X-RAY CLUSTERS	22
<i>The cosmological mass function</i>	22
<i>Deriving Ω_m from cluster evolution</i>	24
OUTLOOK AND FUTURE WORK	27

1 INTRODUCTION

Galaxy clusters arise from the gravitational collapse of rare high peaks of primordial density perturbations in the hierarchical clustering scenario for the formation of cosmic structures (e.g. Peebles 1993, Coles & Lucchin 1995, Peacock 1999). They probe the high-density tail of the cosmic density field and their number density is highly sensitive to specific cosmological scenarios (e.g. Press & Schechter 1974, Kofman et al. 1993, Bahcall & Cen 1993, White et al. 1993a). The space density of clusters in the local universe has been used to measure the amplitude of density perturbations on ~ 10 Mpc scales. Its evolution, which is driven by the growth rate of density fluctuations, essentially depends on the value of the matter density parameter Ω_m ¹ (e.g. Oukbir & Blanchard 1992, Eke et al. 1998, Bahcall et al. 1999). Figure 1 shows how structure formation proceeds and the cluster population evolves in two cosmological models, characterized by different values of Ω_m . High and low density universes show largely different evolutionary patterns, which demonstrate how the space density of distant clusters can be used as a powerful cosmological diagnostic. What cosmological models actually predict is the number density of clusters of a given mass at varying redshifts. The cluster mass, however, is never a directly observable quantity, although several methods exist to estimate it from observations.

Determining the evolution of the space density of clusters requires counting the number of clusters of a given mass per unit volume at different redshifts. Therefore, three essential tools are required for its application as a cosmological test: *i*) an efficient method to find clusters over a wide redshift range; *ii*) an observable estimator of the cluster mass and *iii*) a method to compute the selection function or equivalently the survey volume within which clusters are found.

Clusters form *via* the collapse of cosmic matter over a region of several megaparsecs. Cosmic baryons, which represent approximately 10–15% of the mass content of the Universe, follow the dynamically dominant dark matter during the collapse. As a result of adiabatic compression and of shocks generated by supersonic motions during shell crossing and virialization, a thin hot gas permeating the cluster gravitational potential well is formed. For a typical cluster mass of 10^{14} – $10^{15} M_\odot$ this gas reaches temperatures of several 10^7 K, becomes fully ionized and, therefore, emits via thermal bremsstrahlung in the X-ray band.

Observations of clusters in the X-ray band provide an efficient and physically motivated method of identification, which fulfills the three requirements above. The X-ray luminosity, which uniquely specifies the cluster selection, is also a good probe of the depth of the cluster gravitational potential. For these reasons most of the cosmological studies based on clusters have used X-ray selected samples. X-ray studies of galaxy clusters provide: (1) an efficient way of mapping the

¹The matter-density parameter is defined as $\Omega_m = \bar{\rho}/\rho_c$, where $\bar{\rho}$ is the cosmic mean matter density; $\rho_c = 1.88 \cdot 10^{-29} h^2 \text{ g cm}^{-3}$ is the critical density; h and h_{50} denote the Hubble constant H_0 respectively in units of 100 and 50 km s⁻¹ Mpc⁻¹. Ω_Λ is referred to as the contribution to the total mass-energy density of the Universe associated with the cosmological constant Λ .

overall structure and evolution of the Universe and (2) an invaluable means of understanding their internal structure and the overall history of cosmic baryons.

X-ray cluster studies made substantial progress at the beginning of the 90s with the advent of new X-ray missions. Firstly, the all-sky survey and the deep pointed observations conducted by the *ROSAT* satellite have been a goldmine for the discovery of hundreds of new clusters in the nearby and distant Universe. Follow-up studies with *ASCA* and *Beppo-SAX* satellites revealed hints of the complex physics governing the intra-cluster gas. In addition to gas heating associated with gravitational processes, star formation processes and energy feedback from supernovae and galactic nuclear activity are now understood to play an important role in determining the thermal history of the intra-cluster medium (ICM), its X-ray properties and its chemical composition. Studies utilizing the current new generation of X-ray satellites, *Chandra* and *Newton-XMM*, are radically changing our X-ray view of clusters. The large collecting area of *Newton-XMM*, combined with the superb angular resolution of *Chandra*, have started to unveil the interplay between the complex physics of the hot ICM and detailed processes of star formation associated with cool baryons.

The aim of this article is to provide an up-to-date review on the methodology used to construct X-ray selected cluster samples and to investigate their evolutionary properties. We emphasize the evolution of the space density of clusters and their physical parameters. Additional reviews on galaxy clusters include: Forman & Jones (1982) and Sarazin (1988) for historical reviews on X-ray properties of galaxy clusters; Bahcall (1988) and Borgani & Guzzo (2001) for large-scale structure studies of galaxy clusters; Fabian (1994) for the physics of cooling flows in clusters; Mulchaey (2000) for the X-ray properties of galaxy groups; Birkinshaw (1999) and Carlstrom et al. (2001) for cluster studies with the Sunyaev-Zeldovich effect; Mellier (1999) for studies of the mass distribution of clusters via gravitational lensing and van Dokkum & Franx (2001) for the study of galaxy populations in clusters.

2 PHYSICAL PROPERTIES OF GALAXY CLUSTERS

Clusters of galaxies were first identified as large concentrations in the projected galaxy distribution (Abell 1958, Zwicky et al. 1966, Abell et al. 1989), containing hundreds to thousands galaxies, over a region of the order of ~ 1 Mpc. The first observations showed that such structures are associated with deep gravitational potential wells, containing galaxies with a typical velocity dispersion along the line-of-sight of $\sigma_v \sim 10^3 \text{ km s}^{-1}$. The crossing time for a cluster of size R can be defined as

$$t_{\text{cr}} = \frac{R}{\sigma_v} \simeq 1 \left(\frac{R}{1 \text{ Mpc}} \right) \left(\frac{\sigma_v}{10^3 \text{ km s}^{-1}} \right)^{-1} \text{ Gyr}. \quad (1)$$

Therefore, in a Hubble time, $t_H \simeq 10 h^{-1} \text{ Gyr}$, such a system has enough time in its internal region, $\lesssim 1 h^{-1} \text{ Mpc}$, to dynamically relax – a condition that can not be attained in the surrounding, $\sim 10 \text{ Mpc}$, environment. Assuming virial equilibrium, the typical cluster mass is

$$M \simeq \frac{R\sigma_v^2}{G} \simeq \left(\frac{R}{1 h^{-1} \text{ Mpc}} \right) \left(\frac{\sigma_v}{10^3 \text{ km s}^{-1}} \right)^2 10^{15} h^{-1} M_{\odot}. \quad (2)$$

Smith (1936) first noticed in his study of the Virgo cluster that the mass implied by cluster galaxy motions was largely exceeding that associated with the

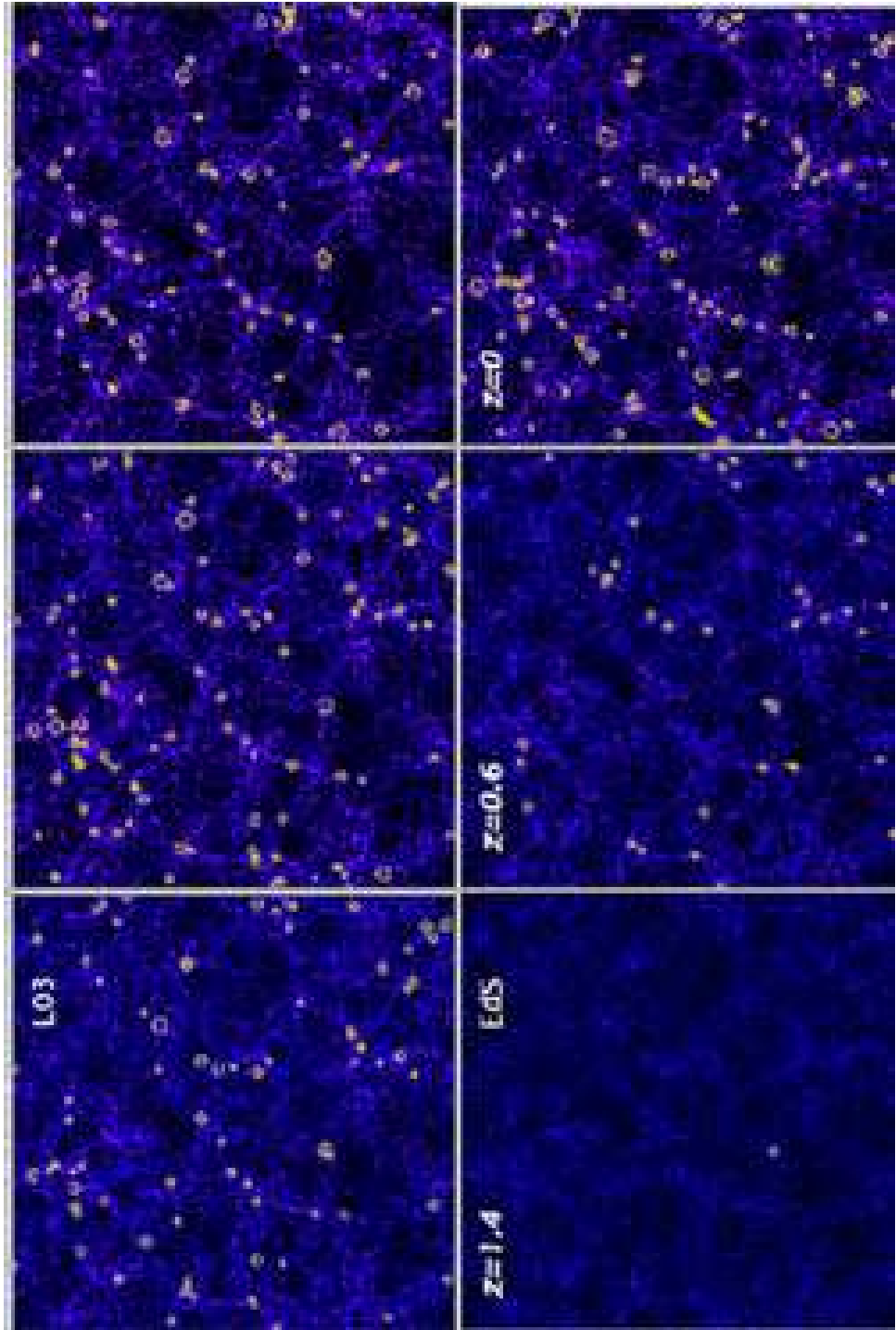


Figure 1: The evolution of the cluster population from N-body simulations in two different cosmologies (from Borgani & Guzzo 2001). Left panels describe a flat, low-density model with $\Omega_m = 0.3$ and $\Omega_\Lambda = 0.7$ (L03); right panels are for an Einstein-de-Sitter model (EdS) with $\Omega_m = 1$. Superimposed on the dark matter distribution, the yellow circles mark the positions of galaxy clusters with virial temperature $T > 3$ keV, the size of the circles is proportional to temperature. Model parameters have been chosen to yield a comparable space density of nearby clusters. Each snapshot is $250h^{-1}$ Mpc across and $75h^{-1}$ Mpc thick (comoving with the cosmic expansion).

optical light component. This was confirmed by Zwicky (1937), and was the first evidence of the presence of dark matter.

2.1 X-ray properties of clusters

Observations of galaxy clusters in the X-ray band have revealed a substantial fraction, $\sim 15\%$, of the cluster mass to be in the form of hot diffuse gas, permeating its potential well. If this gas shares the same dynamics as member galaxies, then it is expected to have a typical temperature

$$k_B T \simeq \mu m_p \sigma_v^2 \simeq 6 \left(\frac{\sigma_v}{10^3 \text{ km s}^{-1}} \right)^2 \text{ keV}, \quad (3)$$

where m_p is the proton mass and μ is the mean molecular weight ($\mu = 0.6$ for a primordial composition with a 76% fraction contributed by hydrogen). Observational data for nearby clusters (e.g. Wu et al. 1999) and for distant clusters (see Figure 2) actually follow this relation, although with some scatter and with a few outliers. This correlation indicates that the idealized picture of clusters as relaxed structures in which both gas and galaxies feel the same dynamics is a reasonable representation. There are some exceptions that reveal the presence of a more complex dynamics.

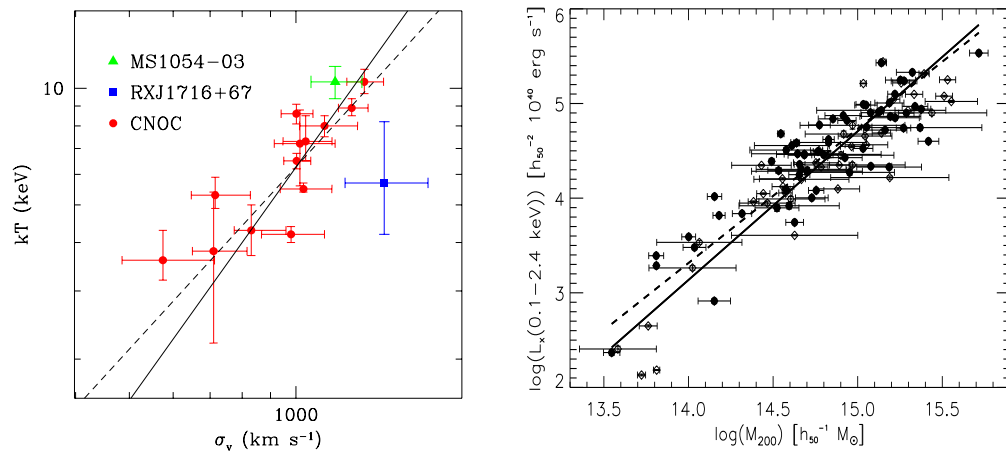


Figure 2: *Left* The relation between galaxy velocity dispersion, σ_v , and ICM temperature, T , for distant ($z > 0.15$) galaxy clusters. Velocity dispersions are taken from Carlberg et al. (1997a) for CNOc clusters and from Girardi & Mezzetti (2001) for MS1054-03 and RXJ1716+67. Temperatures are taken from Lewis et al. (1999) for CNOc clusters, from Jeltema et al. (2001) for MS1054-03 and from Gioia et al. (1999) for RXJ1716+67. The solid line shows the relation $k_B T = \mu m_p \sigma_v^2$, and the dashed line is the best-fit to the low- z T - σ_v relation from Wu et al. (1999). *Right* The low- z relation between X-ray luminosity and the mass contained within the radius encompassing an average density $200\rho_c$ (from Reiprich & Böhringer 2002). The two lines are the best log-log linear fit to two different data sets indicated with filled and open circles.

At the high energies implied by Equation 3, the ICM behaves as a fully ionized

plasma, whose emissivity is dominated by thermal bremsstrahlung. The emissivity for this process at frequency ν scales as $\epsilon_\nu \propto n_e n_i g(\nu, T) T^{-1/2} \exp(-h\nu/k_B T)$, where n_e and n_i are the number density of electrons and ions, respectively, and $g(\nu, T) \propto \ln(k_B T/h\nu)$ is the Gaunt factor. Whereas the pure bremsstrahlung emissivity is a good approximation for $T \gtrsim 3$ keV clusters, a further contribution from metal emission lines should be taken into account when considering cooler systems (e.g. Raymond & Smith 1977). By integrating the above equation over the energy range of the X-ray emission and over the gas distribution, one obtains X-ray luminosities $L_X \sim 10^{43} - 10^{45} \text{ erg s}^{-1}$. These powerful luminosities allow clusters to be identified as extended sources out to large cosmological distances.

Assuming spherical symmetry, the condition of hydrostatic equilibrium connects the local gas pressure p to its density ρ_{gas} according to

$$\frac{dp}{dR} = -\frac{GM(< R)\rho_{\text{gas}}(R)}{R^2}. \quad (4)$$

By inserting the equation of state for a perfect gas, $p = \rho_{\text{gas}} k_B T / \mu m_p$ into Equation (4), one can express, $M(< R)$, the total gravitating mass within R as

$$M(< R) = -\frac{k_B T R}{G \mu m_p} \left(\frac{d \log \rho_{\text{gas}}}{d \log R} + \frac{d \log T}{d \log R} \right). \quad (5)$$

If R is the virial radius, then at redshift z we have $M \propto R^3 \bar{\rho}_0 (1+z)^3 \Delta_{\text{vir}}(z)$, where $\bar{\rho}_0$ is the mean cosmic density at present time and $\Delta_{\text{vir}}(z)$ is the mean overdensity within a virialized region (see also Equation 13, below). For an Einstein–de-Sitter cosmology, Δ_{vir} is constant and therefore, for an isothermal gas distribution, Equation (5) implies $T \propto M^{2/3} (1+z)$.

Such relations show how quantities, such as ρ_{gas} and T , which can be measured from X-ray observations, are directly related to the cluster mass. Thus, in addition to providing an efficient method to detect clusters, X-ray studies of the ICM allow one to measure the total gravitating cluster mass, which is the quantity predicted by theoretical models for cosmic structure formation.

A popular description of the gas density profile is the β -model,

$$\rho_g(r) = \rho_{g,0} \left[1 + \left(\frac{r}{r_c} \right)^2 \right]^{-3\beta/2}, \quad (6)$$

which was introduced by Cavaliere & Fusco-Femiano (1976; see also Sarazin 1988, and references therein) to describe an isothermal gas in hydrostatic equilibrium within the potential well associated with a King dark-matter density profile. The parameter β is the ratio between kinetic dark-matter energy and thermal gas energy (see Equation 3). This model is a useful guideline for interpreting cluster emissivity, although over limited dynamical ranges. Now, with the *Chandra* and *Newton-XMM* satellites, the X-ray emissivity can be mapped with high angular resolution and over larger scales. These new data have shown that Equation 6 with a unique β value cannot always describe the surface brightness profile of clusters (e.g. Allen et al. 2001).

Kaiser (1986) described the thermodynamics of the ICM by assuming it to be entirely determined by gravitational processes, such as adiabatic compression during the collapse and shocks due to supersonic accretion of the surrounding

gas. As long as there are no preferred scales both in the cosmological framework (i.e. $\Omega_m = 1$ and power-law shape for the power spectrum at the cluster scales), and in the physics (i.e. only gravity acting on the gas and pure bremsstrahlung emission), then clusters of different masses are just a scaled version of each other. Because bremsstrahlung emissivity predicts $L_X \propto M \rho_{\text{gas}} T^{1/2}$, $L_X \propto T_X^2 (1+z)^{3/2}$ or, equivalently $L_X \propto M^{4/3} (1+z)^{7/2}$. Furthermore, if we define the gas entropy as $S = T/n^{2/3}$, where n is the gas density assumed fully ionized, we obtain $S \propto T(1+z)^{-2}$.

It was soon recognized that X-ray clusters do not follow these scaling relations. As we discuss in Section 5, below, the observed luminosity–temperature relation for clusters is $L_X \propto T^3$ for $T \gtrsim 2$ keV, and possibly even steeper for $T \lesssim 1$ keV groups. This result is consistent with the finding that $L_X \propto M^\alpha$ with $\alpha \simeq 1.8 \pm 0.1$ for the observed mass–luminosity relation (e.g. Reiprich & Böhringer 2002; see right panel of Figure 2). Furthermore, the low-temperature systems are observed to have shallower central gas-density profiles than the hotter systems, which turns into an excess of entropy in low- T systems with respect to the $S \propto T$ predicted scaling (e.g. Ponman et al. 1999, Lloyd–Davies et al. 2000).

A possible interpretation for the breaking of the scaling relations assumes that the gas has been heated at some earlier epoch by feedback from a non-gravitational astrophysical source (Evrard & Henry 91). This heating would increase the entropy of the ICM, place it on a higher adiabat, prevent it from reaching a high central density during the cluster gravitational collapse and, therefore, decrease the X-ray luminosity (e.g. Balogh et al. 1999, Tozzi & Norman 2001, and references therein). For a fixed amount of extra energy per gas particle, this effect is more prominent for poorer clusters, i.e. for those objects whose virial temperature is comparable with the extra-heating temperature. As a result, the self-similar behavior of the ICM is expected to be preserved in hot systems, whereas it is broken for colder systems. Both semi-analytical works (e.g. Cavaliere et al. 1998, Balogh et al. 1999, Wu et al. 2000; Tozzi et al. 2001) and numerical simulations (e.g. Navarro et al. 1995, Brighenti & Mathews 2001, Bialek et al. 2001, Borgani et al. 2001a) converge to indicate that ~ 1 keV per gas particle of extra energy is required. A visual illustration of the effect of pre-heating is reported in Figure 3, which shows the entropy map for a high-resolution simulation of a system with mass comparable to that of the Virgo cluster, for different heating schemes (Borgani et al. 2001b). The effect of extra energy injection is to decrease the gas density in central cluster regions and to erase the small gas clumps associated with accreting groups.

The gas-temperature distributions in the outer regions of clusters are not affected by gas cooling. These temperature distributions have been studied with the *ASCA* and *Beppo-SAX* satellites. General agreement about the shape of the temperature profiles has still to be reached (e.g. Markevitch et al. 1998, White 2000, Irwin & Bregman 2000). De Grandi & Molendi (2002) analyzed a set of 21 clusters with *Beppo-SAX* data and found the gas to be isothermal out to $\sim 0.2R_{\text{vir}}$, with a significant temperature decline at larger radii. Such results are not consistent with the temperature profiles obtained from cluster hydrodynamical simulations (e.g. Evrard et al. 1996), thus indicating that some physical process is still lacking in current numerical descriptions of the ICM. Deep observations with *Newton-XMM* and *Chandra* will allow the determination of temperature profiles over the whole cluster virialized region.

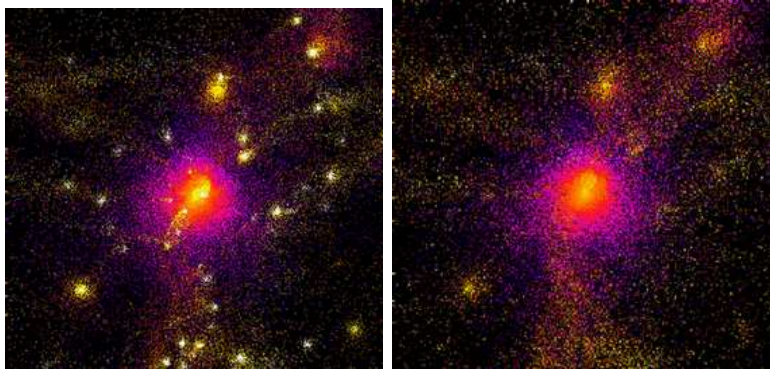


Figure 3: Map of gas entropy from hydrodynamical simulations of a galaxy cluster (from Borgani et al. 2001a). (*Left*): gravitational heating only. (*Right*): entropy floor of 50 keV/cm^2 imposed at $z = 3$, corresponding to about 1 keV/part . Light colors correspond to low entropy particles, and dark blue corresponds to high-entropy gas.

X-ray spectroscopy is a powerful means for analyzing the metal content of the ICM. Measurements of over 100 nearby clusters have yielded a mean metallicity $Z \sim 1/3Z_{\odot}$, largely independent of the cluster temperature (e.g. Renzini 1997, and references therein). The spatial distribution of metals has recently been studied in detail with *ASCA* and *Beppo-SAX* data (e.g. White 2000, De Grandi & Molendi 2001). This field will receive a major boost over the next few years particularly with *Newton-XMM*, which, with a ten-fold improvement in collecting area and much better angular resolution, will be able to map the distribution of different metals in the ICM, such as Fe, S, Si, O.

2.2 Cooling in the Intra Cluster Medium

In order to characterize the role of cooling in the ICM, it is useful to define the cooling time-scale, which for an emission process characterized by a cooling function $\Lambda_c(T)$, is defined as $t_{cool} = k_B T / (n \Lambda(T))$, n being the number density of gas particles. For a pure bremsstrahlung emission: $t_{cool} \simeq 8.5 \times 10^{10} \text{ yr } (n/10^{-3} \text{ cm}^{-3})^{-1} (T/10^8 \text{ K})^{1/2}$. (e.g. Sarazin 1988). Therefore, the cooling time in central cluster regions can be shorter than the age of the Universe. A substantial fraction of gas undergoes cooling in these regions, and consequently drops out of the hot diffuse, X-ray emitting phase. Studies with the *ROSAT* and *ASCA* satellites indicate that the decrease of the ICM temperature in central regions has been recognized as a widespread feature among fairly relaxed clusters (see Fabian 1994, and references therein). The canonical picture of cooling flows predicted that, as the high-density gas in the cluster core cools down, the lack of pressure support causes external gas to flow in, thus creating a superpositions of many gas phases, each one characterized by a different temperature. Our understanding of the ICM cooling structure is now undergoing a revolution thanks to the much improved spatial and spectral resolution provided by *Newton-XMM*. Recent observations have shown the absence of metal lines associated with gas at temperature $\lesssim 3 \text{ keV}$ (e.g. Peterson et al. 2001, Tamura et al. 2001), in stark contrast with the standard cooling flow prediction for the presence of low-temperature gas (e.g. Böhringer et al. 2002a, Fabian et al. 2001a).

Radiative cooling has been also suggested as an alternative to extra heating to explain the lack of ICM self-similarity (e.g. Bryan 2000, Voit & Bryan 2002). When the recently shocked gas residing in external cluster regions leaves the hot phase and flows in, it increases the central entropy level of the remaining gas. The decreased amount of hot gas in the central regions causes a suppression of the X-ray emission (Pearce et al. 2000, Muanwong et al. 2001). This solution has a number of problems. Cooling in itself is a runaway process, leading to a quite large fraction of gas leaving the hot diffuse phase inside clusters. Analytical arguments and numerical simulations have shown that this fraction can be as large as $\sim 50\%$, whereas observational data indicates that only $\lesssim 10\%$ of the cluster baryons are locked into stars (e.g. Bower et al. 2001, Balogh et al. 2001). This calls for the presence of a feedback mechanisms, such as supernova explosions (e.g. Menci & Cavaliere 2000, Finoguenov et al. 2000, Pipino et al. 2002; Kravtsov & Yepes 2000) or Active Galactic Nuclei (e.g. Valageas & Silk 1999, Wu et al. 2000, Yamada & Fujita 2001), which, given reasonable efficiencies of coupling to the hot ICM, may be able to provide an adequate amount of extra energy to balance overcooling.

3 OBSERVATIONAL FRAMEWORK

3.1 *Optically-based Cluster Surveys*

Abell (1958) provided the first extensive, statistically complete sample of galaxy clusters. Based on pure visual inspection, clusters were identified as enhancements in the galaxy surface density on Palomar Observatory Sky Survey (POSS) plates, by requiring that at least 50 galaxies were contained within a metric radius $R_A = 3h_{50}^{-1}$ Mpc and a predefined magnitude range. Clusters were characterized by their *richness* and estimated distance. The Abell catalog has been for decades the prime source for detailed studies of individual clusters and for characterizing the large scale distribution of matter in the nearby Universe. The sample was later extended to the Southern hemisphere by Corwin and Olowin (Abell, Corwin & Olowin, 1989) by using UK Schmidt survey plates. Another comprehensive cluster catalog was compiled by Zwicky and collaborators (Zwicky et al. 1966), who extended the analysis to poorer clusters using criteria less strict than Abell's in defining galaxy overdensities.

Several variations of the Abell criteria defining clusters were used in an automated and objective fashion when digitized optical plates became available. The Edinburgh-Durham Southern Galaxy Catalog, constructed from the COSMOS scans of UK Schmidt plates around the Southern Galactic Pole, was used to compile the first machine-based cluster catalog (Lumsden et al. 1992). In a similar effort, the Automatic Plate Measuring machine galaxy catalog was used to build a sample of ~ 1000 clusters (Maddox et al. 1990, Dalton et al. 1997).

Projection effects in the selection of cluster candidates have been much debated. Filamentary structures and small groups along the line of sight can mimic a moderately rich cluster when projected onto the plane of the sky. In addition, the background galaxy distribution against which two dimensional overdensities are selected, is far from uniform. As a result, the background subtraction process can produce spurious low-richness clusters during searches for clusters in galaxy catalogs. N-body simulations have been extensively used to build mock galaxy catalogs from which the completeness and spurious fraction of Abell-like samples

of clusters can be assessed (e.g. van Haarlem et al. 1997). All-sky, X-ray selected surveys have significantly alleviated these problems and fueled significant progress in this field as discussed below.

Optical plate material deeper than the POSS was successfully employed to search for more distant clusters with purely visual techniques (Kristian et al. 1978, Couch et al. 1991, Gunn et al. 1986). By using red-sensitive plates, Gunn and collaborators were able to find clusters out to $z \simeq 0.9$. These searches became much more effective with the advent of CCD imaging. Postman et al. (1996) were the first to carry out a V&I-band survey over 5 deg^2 (the Palomar Distant Cluster Survey, PDCS) and to compile a sample of 79 cluster candidates using a matched-filter algorithm. This technique enhances the contrast of galaxy overdensities at a given position, utilizing prior knowledge of the luminosity profile typical of galaxy clusters. Olsen et al. (1999) used a similar algorithm to select a sample of 35 distant cluster candidates from the ESO Imaging Survey I-band data. A simple and equally effective counts-in-cell method was used by Lidman & Peterson (1996) to select a sample of 104 distant cluster candidates over 13 deg^2 . All these surveys, by using relatively deep I-band data, are sensitive to rich clusters out to $z \sim 1$. A detailed spectroscopic study of one of the most distant clusters at $z = 0.89$ discovered in this way is reported in Lubin et al. (2000).

Dalcanton (1996) proposed another method of optical selection of clusters, in which drift scan imaging data from relatively small telescopes is used to detect clusters as positive surface brightness fluctuations in the background sky. Gonzalez et al. (2001) used this technique to build a sample of ~ 1000 cluster candidates over 130 deg^2 . Spectroscopic follow-up observations will assess the efficiency of this technique.

The advantage of carrying out automated searches based on well-defined selection criteria (e.g. Postman et al. 1996) is that the survey selection function can be computed, thus enabling meaningful statistical studies of the cluster population. For example, one can quantify the probability of detecting a galaxy cluster as a function of redshift for a given set of other parameters, such as galaxy luminosity function, luminosity profile, luminosity and color evolution of cluster galaxies, and field galaxy number counts. A comprehensive report on the performance of different cluster detection algorithms applied to two-dimensional projected distributions can be found in Kim et al. (2002).

The success rate of finding real bound systems in optical surveys is generally relatively high at low redshift ($z < 0.3$, Holden et al. 1999), but it degrades rapidly at higher redshifts, particularly if only one passband is used, as the field galaxy population overwhelms galaxy overdensities associated with clusters. The simplest way to counteract this effect is to observe in the near-infrared bands ($\gtrsim 1 \mu m$). The cores of galaxy clusters are dominated by red, early-type galaxies at least out to $z \simeq 1.3$ for which the dimming effect of the K-correction is particularly severe. In addition, the number counts of the field galaxy population are flatter in the near-IR bands than in the optical. Thus, by moving to z, J, H, K bands, one can progressively compensate the strong K-correction and enhance the contrast of (red) cluster galaxies against the background (blue) galaxy distribution. An even more effective way to enhance the contrast of distant clusters is to use some color information, so that only overdensities of galaxies with peculiar red colors can be selected from the field. With a set of two or three broad band filters, which sample the rest frame UV and optical light at different redshifts, one can separate out early type galaxies which dominate cluster cores from the late type

galaxy population in the field. The position of the cluster red sequence in color-magnitude diagrams, and red clumps in color-color diagrams can also be used to provide an accurate estimate of the cluster redshift, by modeling the relatively simple evolutionary history of early-type galaxies.

The effectiveness of this method was clearly demonstrated by Stanford et al. (1997), who found a significant overdensity of red galaxies with $J - K$ and $I - K$ colors typical of $z > 1$ ellipticals and were able to spectroscopically confirm this system as a cluster at $z = 1.27$ (c.f. see also Dickinson 1997). With a similar color enhancement technique and follow-up spectroscopy, Rosati et al. (1999) confirmed the existence of an X-ray selected cluster at $z = 1.26$. Gladders & Yee (2000) applied the same technique in a systematic fashion to carry out a large area survey in R and z bands (the Red Sequence Survey), which is currently underway and promises to unveil rare, very massive clusters out to $z \sim 1$.

By increasing the number of observed passbands one can further increase the efficiency of cluster selection and the accuracy of their estimated redshifts. In this respect, a significant step forward in mapping clusters in the local Universe will be made with the five-band photometry provided by the Sloan Digital Sky Survey (York et al. 2000). The data will allow clusters to be efficiently selected with photometric redshift techniques, and will ultimately allow hundreds of clusters to be searched directly in redshift space. The next generation of wide field (> 100 deg²) deep multicolor surveys in the optical and especially the near-infrared will powerfully enhance the search for distant clusters.

3.2 X-ray Cluster Surveys

The *Uhuru* X-ray satellite, which carried out the first X-ray sky survey (Giacconi et al. 1972), revealed a clear association between rich clusters and bright X-ray sources (Gursky et al. 1971, Kellogg et al. 1971). *Uhuru* observations also established that X-ray sources identified as clusters were among the most luminous in the sky (10^{43-45} erg s⁻¹), were extended and showed no variability. Felten et al. (1966) first suggested the X-ray originated as thermal emission from diffuse hot intra-cluster gas (Cavaliere et al. 1971). This was later confirmed when the first high quality X-ray spectra of clusters were obtained with the HEAO-1 A2 experiment (e.g. Henriksen and Mushotzsky, 1986). These spectra were best fit by a thermal bremsstrahlung model, with temperatures in the range $2 \times 10^7 - 10^8$ keV, and revealed the 6.8 keV iron K α line, thus showing that the ICM was a highly ionized plasma pre-enriched by stellar processes.

The HEAO-1 X-ray Observatory (Rothschild et al. 1979) performed an all-sky survey with much improved sensitivity compared to *Uhuru* and provided the first flux-limited sample of extragalactic X-ray sources in the 2-10 keV band, with a limiting flux of 3×10^{-11} erg cm⁻² s⁻¹ (Piccinotti et al. 1982). Among the 61 extragalactic sources discovered outside the galactic plane ($|b| > 20^\circ$), 30 were identified as galaxy clusters, mostly in the Abell catalog. This first X-ray flux-limited sample allowed an estimate of the cluster X-ray luminosity function (XLF) in the range $L_X = 10^{43} - 3 \cdot 10^{45}$ erg s⁻¹. The derived space density of clusters (all at $z < 0.1$) is fairly close to current values. An earlier determination of the XLF based on optically selected Abell clusters (McKee et al. 1980) and the same HEAO-1 A2 data gave similar results.

The Piccinotti et al. sample was later augmented by Edge et al. (1990), who extended the sample using the *Ariel V* catalog (McHardy et al. 1981) and revised

the identifications of several clusters using follow-up observations by the *Einstein Observatory* and *EXOSAT*. With much improved angular resolution, these new X-ray missions allowed confused sources to be resolved and fluxes to be improved. The resulting sample included 55 clusters with a flux limit a factor of two fainter than in the original Piccinotti catalog.

Confusion effects in the large beam ($\gtrsim 1^\circ$) early surveys, such as *HEAO-1* and *Ariel V*, had been the main limiting factor in cluster identification. With the advent of X-ray imaging with focusing optics in the 80's, particularly with the *Einstein Observatory* (Giacconi et al. 1979), it was soon recognized that X-ray surveys offer an efficient means of constructing samples of galaxy clusters out to cosmologically interesting redshifts.

First, the X-ray selection has the advantage of revealing physically-bound systems, because diffuse emission from a hot ICM is the direct manifestation of the existence of a potential well within which the gas is in dynamical equilibrium with the cool baryonic matter (galaxies) and the dark matter. Second, the X-ray luminosity is well correlated with the cluster mass (see right panel of Figure 2). Third, the X-ray emissivity is proportional to the square of the gas density (Section 2), hence cluster emission is more concentrated than the optical bidimensional galaxy distribution. In combination with the relatively low surface density of X-ray sources, this property makes clusters high contrast objects in the X-ray sky, and alleviates problems due to projection effects that affect optical selection. Finally, an inherent fundamental advantage of X-ray selection is the ability to define flux-limited samples with well-understood selection functions. This leads to a simple evaluation of the survey volume and therefore to a straightforward computation of space densities. Nonetheless, there are some important caveats described below.

Pioneering work in this field was carried out by Gioia et al. (1990a) and Henry et al. (1992) based on the *Einstein Observatory* Extended Medium Sensitivity Survey (EMSS, Gioia et al. 1990b). The EMSS survey covered over 700 square degrees using 1435 imaging proportional counter (IPC) fields. A highly complete spectroscopic identification of 835 serendipitous sources lead to the construction of a flux-limited sample of 93 clusters out to $z = 0.58$. By extending significantly the redshift range probed by previous samples (e.g. Edge et al. 1990), the EMSS allowed the cosmological evolution of clusters to be investigated. Several follow-up studies have been undertaken such as the CNOC survey (e.g. Yee et al. 1996), and gravitational lensing (Gioia & Luppino 1994).

The *ROSAT* satellite, launched in 1990, allowed a significant step forward in X-ray surveys of clusters. The *ROSAT-PSPC* detector, in particular, with its unprecedented sensitivity and spatial resolution, as well as low instrumental background, made clusters high contrast, extended objects in the X-ray sky. The *ROSAT* All-Sky Survey (RASS, Trümper 1993) was the first X-ray imaging mission to cover the entire sky, thus paving the way to large contiguous-area surveys of X-ray selected nearby clusters (e.g. Ebeling et al. 1997, 1998, 2000, 2001; Burns et al. 1996; Crawford et al. 1995; De Grandi et al. 1999; Böhringer et al. 2000, 2001). In the northern hemisphere, the largest compilations with virtually complete optical identification include, the Bright Cluster Sample (BCS, Ebeling et al. 1998), its extension (Ebeling et al. 2000b), and the Northern *ROSAT* All Sky Survey (NORAS, Böhringer et al. 2000). In the southern hemisphere, the *ROSAT*-ESO flux limited X-ray (REFLEX) cluster survey (Böhringer et al. 2001) has completed the identification of 452 clusters, the largest, homogeneous com-

pilation to date. Another on-going study, the Massive Cluster Survey (MACS, Ebeling et al. 2001) is aimed at targeting the most luminous systems at $z > 0.3$ which can be identified in the RASS at the faintest flux levels. The deepest area in the RASS, the North Ecliptic Pole (NEP, Henry et al. 2001) which *ROSAT* scanned repeatedly during its All-Sky survey, was used to carry out a complete optical identification of X-ray sources over a 81 deg² region. This study yielded 64 clusters out to redshift $z = 0.81$.

In total, surveys covering more than 10⁴ deg² have yielded over 1000 clusters, out to redshift $z \simeq 0.5$. A large fraction of these are new discoveries, whereas approximately one third are identified as clusters in the Abell or Zwicky catalogs. For the homogeneity of their selection and the high degree of completeness of their spectroscopic identifications, these samples are now becoming the basis for a large number of follow-up investigations and cosmological studies.

After the completion of the all-sky survey, *ROSAT* conducted thousands of pointed observations, many of which (typically those outside the galactic plane not targeting very bright or extended X-ray sources) can be used for a serendipitous search for distant clusters. It was soon realized that the good angular resolution of the *ROSAT-PSPC* allowed screening of thousands of serendipitous sources and the selection of cluster candidates *solely* on the basis of their flux and spatial extent. In the central 0.2 deg² of the *PSPC* field of view the point spread function (PSF) is well approximated by a Gaussian with FWHM= 30 – 45". Therefore a cluster with a canonical core radius of 250 h^{-1} kpc (Forman & Jones 1982) should be resolved out to $z \sim 1$, as the corresponding angular distance always exceeds 45" for current values of cosmological parameters (important surface brightness biases are discussed below).

ROSAT-PSPC archival pointed observations were intensively used for serendipitous searches of distant clusters. These projects, which are now completed or nearing completion, include: the RIXOS survey (Castander et al. 1995), the *ROSAT* Deep Cluster Survey (RDCS, Rosati et al. 1995, 1998), the Serendipitous High-Redshift Archival *ROSAT* Cluster survey (SHARC, Collins et al. 1997, Burke et al. 1997), the Wide Angle *ROSAT* Pointed X-ray Survey of clusters (WARPS, Scharf et al. 1997, Jones et al. 1998, Perlman et al. 2002), the 160 deg² large area survey (Vikhlinin et al. 1998b), the *ROSAT* Optical X-ray Survey (ROXS, Donahue et al. 2001). *ROSAT*-HRI pointed observations, which are characterized by a better angular resolution although with higher instrumental background, have also been used to search for distant clusters in the Brera Multi-scale Wavelet catalog (BMW, Campana et al. 1999).

A principal objective of all these surveys has been the study of the cosmological evolution of the space density of clusters. Results are discussed in Section 4 and 5, below. In Figure 4, we give an overview of the flux limits and surveyed areas of all major cluster surveys carried out over the last two decades. RASS-based surveys have the advantage of covering contiguous regions of the sky so that the clustering properties of clusters (e.g. Collins et al. 2000, Mullis et al. 2001), and the power spectrum of their distribution (Schücker et al. 2001a) can be investigated. They also have the ability to unveil rare, massive systems albeit over a limited redshift and X-ray luminosity range. Serendipitous surveys, or general surveys, which are at least a factor of ten deeper but cover only a few hundreds square degrees, provide complementary information on lower luminosities, more common systems and are well suited for studying cluster evolution on a larger redshift baseline. The deepest pencil-beam surveys, such as the Lockman Hole

with *XMM* (Hasinger et al. 2000) and the Chandra Deep Fields (Giacconi et al. 2002, Bauer et al. 2002), allow the investigation of the faintest end of the XLF (poor clusters and groups) out to $z \sim 1$.

3.3 Strategies and Selection Functions for X-ray Surveys

Ideally, one would like to use selection criteria based on X-ray properties alone to construct a flux-limited sample with a simple selection function. The task of separating clusters from the rest of the X-ray source population is central to this work. At the *ROSAT* flux limit ($\sim 1 \times 10^{-14}$ erg cm $^{-2}$ s $^{-1}$ for clusters) $\sim 10\%$ of extragalactic X-ray sources are galaxy clusters. A program of complete optical identification is very time consuming, as only spectroscopy can establish in many cases whether the X-ray source is associated with a real cluster. The EMSS and NEP samples, for example, were constructed in this way. In some cases, the hardness ratio (a crude estimate of the source's X-ray spectral energy distribution) is used to screen out sources which are incompatible with thermal spectra or to resolve source blends. With the angular resolution provided by *ROSAT*, however, it became possible to select clusters on the basis of their spatial extent. This is particularly feasible with pointed observations, as opposed to all-sky survey data which are characterized by a broader PSF and shallower exposures, so that faint and/or high redshift clusters are not always detected as extended (e.g. Ebeling et al. 1997, Böhringer et al. 2001).

In constructing RASS based samples (shaded circles in Figure 4) most of the authors had to undertake a complete optical identification program of $\sim 10^4$ sources using POSS plates or CCD follow-up imaging in order to build a sample of cluster candidates. Whereas a sizable fraction of these systems can be readily identified in previous cluster catalogs (primarily Abell's), spectroscopy is needed to measure redshifts of newly discovered systems or to resolve ambiguous identifications. We recall that optically selected, X-ray confirmed samples, such as the X-ray Brightest Abell-like Clusters (XBACS, Ebeling et al. 1996), while useful for studying optical-X-ray correlations, lead to incomplete flux-limited samples. Many of the low X-ray luminosity systems (poor clusters or groups) are missed in the optical selection even though they lie above the X-ray flux limit of the RASS.

Most of the *ROSAT* serendipitous surveys (dark circles in Figure 4) have adopted a very similar methodology but somewhat different identification strategies. Cluster candidates are selected from a serendipitous search for extended X-ray sources above a given flux limit in deep *ROSAT*-PSPC pointed observations. Moderately deep CCD imaging in red passbands (or in near-IR for the most distant candidates) is used to reveal galaxy overdensities near the centroid of X-ray emission. Extensive spectroscopic follow-up programs associated with these surveys, have led to the identification of roughly 200 new clusters or groups, and have increased the number of clusters known at $z > 0.5$ by approximately a factor of ten.

An essential ingredient for the evaluation of the selection function of X-ray surveys is the computation of the sky coverage: the effective area covered by the survey as a function of flux. In general, the exposure time, as well as the background and the PSF are not uniform across the field of view of X-ray telescopes (owing to their inherent optical design), which introduces vignetting and a degradation of the PSF at increasing off-axis angles. As a result, the sensitivity to source detection varies significantly across the survey area so that only bright

sources can be detected over the entire solid angle of the survey, whereas at faint fluxes the effective area decreases. An example of survey sky coverage is given in Figure 5 (left). By integrating the volume element of the Friedmann-Robertson-Walker metric, $dV/d\Omega dz(z, \Omega_m, \Omega_\Lambda)$ (e.g. Carroll et al. 1992), over these curves one can compute the volume that each survey probes above a given redshift z , for a given X-ray luminosity ($L_X = 3 \times 10^{44} \text{ erg s}^{-1} \simeq L_X^*$, the characteristic luminosity, in the figure). The resulting survey volumes are shown in Figure 5 (right). By normalizing this volume to the local space density of clusters (ϕ^* , see below) one obtains the number of L^* volumes accessible in the survey above a given redshift. Assuming no evolution, this yields an estimate of the number of typical bright clusters one expects to discover.

By covering different solid angles at varying fluxes, these surveys probe different volumes at increasing redshift and therefore different ranges in X-ray luminosities at varying redshifts. The EMSS has the greatest sensitivity to the most luminous, yet rare, systems but only a few clusters at high redshift lie above its bright flux limit. Deep *ROSAT* surveys probe instead the intermediate-to-faint end of the XLF. As a result, they have led to the discovery of many new clusters at $z > 0.4$. The RDCS has pushed this search to the faintest fluxes yet, providing sensitivity to the highest redshift systems with $L_X \lesssim L_X^*$ even beyond $z = 1$. The WARPS, and particularly the 160 deg² survey have covered larger areas at high fluxes thus better studying the bright end of the XLF out to $z \simeq 1$.

Particular emphasis is given in these searches to detection algorithms that are designed to examine a broad range of cluster parameters (X-ray flux, surface brightness, morphology) and to deal with source confusion at faint flux levels. The traditional detection algorithm used in X-ray astronomy for many years, the sliding cell method, is not adequate for this purpose. A box of fixed size is slid across the image, and sources are detected as positive fluctuations that deviate significantly from Poissonian expectations based on a global background map (the latter being constructed from a first scan of the image). Although this method works well for point-like sources, it is less suited to extended, low-surface brightness sources, which can consequently be missed leading to a significant incompleteness in flux-limited cluster samples.

The need for more general detection algorithms, not only geared to the detection of point sources, became important with *ROSAT* observations, which probe a much larger range in surface brightness than previous missions (e.g. *Einstein*). A popular alternative approach to source detection and characterization developed specifically for cluster surveys is based on wavelet techniques (e.g. Rosati et al. 1995, Vikhlinin et al. 1998b, Lazzati et al. 1999, Romer et al. 2000). Wavelet analysis is essentially a multi-scale analysis of the image based on a quasi-orthonormal decomposition of a signal via the wavelet transform which enables significant enhancement of the contrast of sources of different sizes against non-uniform backgrounds. This method, besides being equally efficient at detecting sources of different shapes and surface brightnesses, is well-suited to dealing with confusion effects, and allows source parameters to be measured without knowledge of the background. Another method that has proved to be well-suited for the detection of extended and low surface brightness emission is based on Voronoi Tessellation and Percolation (VTP, Scharf et al. 1997 and references therein).

Besides detection algorithms, which play a central role in avoiding selection ef-

fects, there are additional caveats to be considered when computing the selection function of X-ray cluster surveys. For example, the sky coverage function (Figure 5) depends not only on the source flux but in general on the extent or surface brightness of cluster sources (Rosati et al. 1995, Scharf et al. 1997, Vikhlinin et al. 1998). This effect can be tested with extensive simulations, by placing artificial clusters (typically using β -profiles) in the field and measuring the detection probability for different cluster parameters or instrumental parameters.

More generally, as in all flux-limited samples of extended sources (e.g. optical galaxy surveys), one has to make sure that the sample does not become surface brightness (SB) limited at very faint fluxes. As the source flux decreases, clusters with smaller mean SB have a higher chance of being missed, because their signal-to-noise is likely to drop below the detection threshold. SB dimming at high redshifts ($SB \propto (1+z)^{-4}$) can thus create a serious source of incompleteness at the faintest flux levels. This depends critically on the steepness of the SB-profile of distant X-ray clusters, and its evolution. Besides simulations of the detection process, the most meaningful way to test these selection effects is to verify that derived cluster surface or space densities do not show any trend across the survey area (e.g. a decrease in regions with higher background, low exposures, degraded PSF). The task of the observer is to understand what is the fiducial flux limit above which the sample is truly flux-limited and free of SB effects. This fiducial flux limit is typically a factor of 2–3 higher than the minimum detectable flux in a given survey.

An additional source of sample contamination or misidentification may be caused by clusters hosting X-ray bright AGN, or by unrelated point sources projected along the line of sight of diffuse cluster emission. The former case does not seem to be a matter of great concern, because bright AGN have been found near the center of clusters in large compilations (Böhringer et al. 2001) in less than 5% of the cases. The latter effect can be significant in distant and faint *ROSAT* selected clusters, for which high resolution *Chandra* observations (Stanford et al. 2001, 2002) have revealed up to 50% flux contamination in some cases.

Concerning selection biases, a separate issue is whether, using X-ray selection, one might miss systems that, although virialized, have an unusually low X-ray luminosity. These systems would be outliers in the $L_X - M$ or $L_X - T$ relation (Section 5.2). Such hypothetical systems are at odds with our physical understanding of structure formation and would require unusual mechanisms that would (a) lead galaxies to virialize but the gaseous component not to thermalize in the dark matter potential well, (b) allow energy sources to dissipate or remove the gas after collapse, or (c) involve formation scenarios in which only a small fraction of the gas collapses. Similarly, systems claimed to have unusually high mass-to-optical luminosity ratio, M/L , such as MG2016+112 from *ASCA* observations (Hattori et al. 1998) have not held up. MG2016+112 was later confirmed to be an ordinary low mass cluster at $z = 1$ by means of near-infrared imaging (Benitez et al. 1999) and spectroscopic (Soucail et al. 2001) follow-up studies. Chartas et al. (2001) have completely revised the nature of the X-ray emission with *Chandra* observations. Comparing optical and X-ray techniques for clusters' detection, Donahue et al. (2001) carried out an optical/X-ray joint survey in the same sky area (ROXS). They found no need to invoke an X-ray faint population of massive clusters.

3.4 Other methods

X-ray and optical surveys have been by far the most exploited techniques for studying the distribution and evolution of galaxy clusters. It is beyond the scope of this paper to review other cluster-finding methods, which we only summarize here for completeness:

- *Search for galaxy overdensities around high- z radio galaxies or AGN*: searches are conducted in near-IR or narrow-band filters, or by means of follow-up X-ray observations. Although not suited for assessing cluster abundances, this method has provided the only examples of possibly virialized systems at $z > 1.5$ (e.g. Pascarelle et al. 1996; Dickinson 1997; Crawford & Fabian 1996, Hall & Green 1998; Pentericci et al. 2000; Fabian et al. 2001b, Venemans et al. 2002).
- *Sunyaev-Zeldovich effect*: clusters are revealed by measuring the distortion of the CMB spectrum owing to the hot ICM. This method does not depend on redshift and provides reliable estimate of cluster masses. It is possibly one of the most powerful methods to find distant clusters in the years to come. At present, serendipitous surveys with interferometric techniques (e.g. Carlstrom et al. 2001) cannot cover large areas (i.e. more than ~ 1 deg²) and their sensitivity is limited to the most X-ray luminous clusters.
- *Gravitational lensing*: in principle a powerful method to discover mass concentrations in the universe through the statistical distortion of background galaxy images (see Mellier 1999 for a review).
- *Search for clusters around bent-double radio sources*: radio galaxies with bent lobes are often associated with dense ICM and are therefore good tracers of rich cluster environments (e.g. Blanton et al. 2001).
- *Clustering of absorption line systems*: this method has lead to a few detections of “proto-clusters” at $z \gtrsim 2$ (e.g. Francis et al. 1996). The most serious limitation of this technique is the small sample volume.

4 THE SPACE DENSITY OF X-RAY CLUSTERS

4.1 Local Cluster Number Density

The determination of the local ($z \lesssim 0.3$) cluster abundance plays a crucial role in assessing the evolution of the cluster abundance at higher redshifts. The cluster XLF is commonly modeled with a Schechter function:

$$\phi(L_X)dL_X = \phi^* \left(\frac{L_X}{L_X^*} \right)^{-\alpha} \exp(-L_X/L_X^*) \frac{dL_X}{L_X^*}, \quad (7)$$

where α is the faint-end slope, L_X^* is the characteristic luminosity, and ϕ^* is directly related to the space-density of clusters brighter than L_{min} : $n_0 = \int_{L_{min}}^{\infty} \phi(L)dL$. The cluster XLF in the literature is often written as: $\phi(L_{44}) = K \exp(-L_X/L_X^*) L_{44}^{-\alpha}$, with $L_{44} = L_X/10^{44} \text{ erg s}^{-1}$. The normalization K , expressed in units of $10^{-7} \text{ Mpc}^{-3} (10^{44} \text{ erg s}^{-1})^{\alpha-1}$, is related to ϕ^* by $\phi^* = K (L_X^*/10^{44})^{1-\alpha}$.

Using a flux-limited cluster sample with measured redshifts and luminosities, a binned representation of the XLF can be obtained by adding the contribution

to the space density of each cluster in a given luminosity bin ΔL_X :

$$\phi(L_X) = \left(\frac{1}{\Delta L_X} \right) \sum_{i=1}^n \frac{1}{V_{max}(L_i, f_{lim})}; \quad (8)$$

where V_{max} is the total search volume defined as

$$V_{max} = \int_0^{z_{max}} S[f(L, z)] \left(\frac{d_L(z)}{1+z} \right)^2 \frac{c dz}{H(z)}. \quad (9)$$

Here $S(f)$ is the survey sky coverage, which depends on the flux $f = L/(4\pi d_L^2)$, $d_L(z)$ is the luminosity distance, and $H(z)$ is the Hubble constant at z (e.g. Peebles 1993, pag.312). We define z_{max} as the maximum redshift out to which the object is included in the survey. Equations 8 and 9 can be easily generalized to compute the XLF in different redshift bins.

In Figure 6 we summarize the recent progress made in computing $\phi(L_X)$ using primarily low-redshift *ROSAT* based surveys. This work improved the first determination of the cluster XLF (Piccinotti et al. 1982, see Section 3.2). The BCS and REFLEX cover a large L_X range and have good statistics at the bright end, $L_X \gtrsim L_X^*$ and near the knee of the XLF. Poor clusters and groups ($L_X \lesssim 10^{43}$ erg s $^{-1}$) are better studied using deeper surveys, such as the RDCS. The very faint end of the XLF has been investigated using an optically selected, volume-complete sample of galaxy groups detected *a posteriori* in the RASS (Burns et al. 1996).

From Figure 6, we note the very good agreement among all these independent determinations. Best-fit parameters are consistent with each other with typical values: $\alpha \simeq 1.8$ (with 15% variation), $\phi^* \simeq 1 \times 10^{-7} h_{50}^3 \text{Mpc}^{-3}$ (with 50% variation), and $L_X^* \simeq 4 \times 10^{44}$ erg s $^{-1}$ [0.5–2 keV]. Residual differences at the faint end are probably the result of cosmic variance effects, because the lowest luminosity systems are detected at very low redshifts where the search volume becomes small (see Böhringer et al. 2002b). Such an overall agreement is quite remarkable considering that all these surveys used completely different selection techniques and independent datasets. Evidently, systematic effects associated with different selection functions are relatively small in current large cluster surveys. This situation is in contrast with that for the galaxy luminosity function in the nearby Universe, which is far from well established (Blanton et al. 2001). The observational study of cluster evolution has indeed several advantages respect to galaxy evolution, despite its smaller number statistics. First, a robust determination of the local XLF eases the task of measuring cluster evolution. Second, X-ray spectra constitute a single parameter family based on temperature and K-corrections are much easier to compute than in the case of different galaxy types in the optical bands.

4.2 The Cluster Abundance at Higher Redshifts and Its Evolution

A first analysis of the EMSS cluster sample (Gioia et al. 1990a) revealed negative evolution of the XLF – a steepening of the high-end of XLF indicating a dearth of high luminosity clusters at $z > 0.3$. This result was confirmed by Henry et al. (1992) using the complete EMSS sample with an appropriate sky coverage function. Edge et al. (1990) found evidence of a strong negative evolution already at redshifts < 0.2 using a HEAO-1 based cluster sample (see Section 3.2). The

very limited redshift baseline made this result somewhat controversial, until it was later ruled out by the analysis of the first RASS samples (Ebeling et al. 1997). The *ROSAT* deep surveys extended the EMSS study on cluster evolution. Early results (Castander et al. 1995) seemed to confirm and even to reinforce the evidence of negative evolution. This claim, based on a sample of 12 clusters, was later recognized to be the result of sample incompleteness and an overestimate of the solid angle covered at low fluxes and its corresponding search volume (Burke et al. 1997, Rosati et al. 1998, Jones et al. 1998).

If cluster redshifts are not available, X-ray flux-limited samples can be used to trace the surface density of clusters at varying fluxes. In Figure 7, we show several determinations of the cumulative cluster number counts stretching over five decades in flux. This comparison shows a good agreement (at the 2σ level) among independent determinations (see also Gioia et al. 2001). The slope at bright fluxes is very close to the Euclidean value of 1.5 (as expected for an homogeneous distribution of objects over large scales), whereas it flattens to $\simeq 1$ at faint fluxes. The slope of the $\text{Log}N\text{--Log}S$ is mainly determined by the faint-to-moderate part of the XLF, but it is rather insensitive to the abundance of the most luminous, rare systems. The fact that the observed counts are consistent with no-evolution predictions, obtained by integrating the local XLF, can be interpreted as an indication that a significant fraction of the cluster population does not evolve with redshift (Rosati et al. 1995, 1998, Jones et al. 1998, Vikhlinin et al. 1998a). We have included the recent data from the Chandra Deep Fields North (Bauer et al. 2002) and South (Giacconi et al. 2002), which have extended the number counts by two decades. Note that cosmic variance may be significant because these are only two, albeit deep, pencil beam fields ($\lesssim 0.1 \text{ deg}^2$). Serendipitous surveys with *Chandra* and *XMM* (see Figure 4) will fill the gap between these measurements and the *ROSAT* surveys. The no evolution curves in Figure 7 are computed by integrating the BCS local XLF (Ebeling et al. 1997) according to the evolutionary model in Figure 9.

A much improved picture of the evolution of the cluster abundance emerged when, with the completion of spectroscopic follow-up studies, several cluster samples were used to compute the XLF out to $z \simeq 0.8$. These first measurements are summarized in Figure 8. Although binned representations of the XLF are not straightforward to compare, it is evident that within the error bars there is little, if any, evolution of the cluster space density at $L_X([0.5 - 2]\text{keV}) \lesssim 3 \times 10^{44} \text{ erg s}^{-1} \simeq L_X^*$ out to redshift $z \simeq 0.8$. These results (Burke et al. 1997, Rosati et al. 1998, Jones et al. 1998, Vikhlinin et al. 1998a, Nichols et al. 1999) extended the original study of EMSS to fainter luminosities and larger redshifts, and essentially confirmed the EMSS findings in the overlapping X-ray luminosity range. The ability of all these surveys to adequately study the bright end of the XLF is rather limited, since there is not enough volume to detect rare systems with $L_X > L_X^*$. The 160 deg^2 survey by Vikhlinin et al. (1998a), with its large area, did however confirm the negative evolution at $L_X \gtrsim 4 \times 10^{44} \text{ erg s}^{-1}$. Further analyses of these datasets have confirmed this trend, i.e. an apparent drop of super- L_X^* clusters at $z \gtrsim 0.5$ (Nichol et al. 1999 from the Bright-SHARC survey; Rosati et al. 2000 from the RDCS, Gioia et al. 2001 from the NEP survey). These findings, however, were not confirmed by Ebeling et al. (2000) in an analysis of the WARPS sample.

The evolution of the bright end of the XLF has remained a hotly debated sub-

ject for several years. The crucial issue in this debate is to properly quantify the statistical significance of any claimed evolutionary effect. The binned representation of the XLF in Figure 8 can be misleading and can even lead to biases (Page & Carrera 2000). The full information contained in any flux-limited cluster sample can be more readily recovered by analyzing the unbinned (L_X, z) distribution with a maximum-likelihood approach, which compares the observed cluster distribution on the (L_X, z) plane with that expected from a given XLF model. Rosati et al. (2000) used this method by modeling the cluster XLF as an evolving Schechter function: $\phi(L) = \phi_0(1+z)^A L^{-\alpha} \exp(-L/L^*)$, with $L^* = L_0^*(1+z)^B$; where A and B are two evolutionary parameters for density and luminosity; ϕ_0 and L_0^* the local XLF values (Equation 7). Figure 9 shows an application of this method to the RDCS and EMSS sample, and indicates that the no-evolution case ($A = B = 0$) is excluded at more than 3σ levels in both samples when the most luminous systems are included in the analysis. However, the same analysis confined to clusters with $L_X < 3 \times 10^{44}$ erg s $^{-1}$ yields an XLF consistent with no evolution. In Figure 9 we also report the latest determinations of the XLF out to $z \sim 1$.

In summary, by combining all the results from *ROSAT* surveys one obtains a consistent picture in which the comoving space density of the bulk of the cluster population is approximately constant out to $z \simeq 1$, but the most luminous ($L_X \gtrsim L_X^*$), presumably most massive clusters were likely rarer at high redshifts ($z \gtrsim 0.5$). Significant progress in the study of the evolution of the bright end of the XLF would require a large solid angle and a relatively deep survey with an effective solid angle of $\gg 100$ deg 2 at a limiting flux of 10^{-14} erg cm $^{-2}$ s $^{-1}$.

The convergence of the results from several independent studies illustrates remarkable observational progress in determining the abundance of galaxy clusters out to $z \sim 1$. At the beginning of the *ROSAT* era, until the mid nineties, controversy surrounded the usefulness of X-ray surveys of distant galaxy clusters and many believed that clusters were absent at $z \sim 1$. This prejudice arose from an over-interpretation of the early results of the EMSS survey. Gioia et al. (1990a) did point out that the evolution of the XLF was limited only to the very luminous systems but this important caveat was often overlooked. The original controversy concerning cluster evolution inferred from optical and X-ray data finds an explanation in light of the *ROSAT* results. Optical surveys (Couch et al. 1991, Postman et al. 1996) have shown no dramatic decline in the comoving volume density of rich clusters out to $z \simeq 0.5$. This was considered to be in contrast with the EMSS findings. However, these optical searches covered limited solid angles (much smaller than the EMSS) and therefore did not probe adequately the seemingly evolving high end of the cluster mass function.

4.3 Distant X-ray Clusters: the Latest View from Chandra

With its unprecedented angular resolution, the *Chandra* satellite has revolutionized X-ray astronomy, allowing studies with the same level of spatial details as in optical astronomy. *Chandra* imaging of low redshift clusters has revealed a complex thermodynamical structure of the ICM down to kiloparsec scales (e.g. Markevitch et al. 2000, Fabian et al. 2000). At high redshifts, deep *Chandra* images still have the ability to resolve cluster cores and to map ICM morphologies at scales below 100 kpc. Moreover, temperatures of major subclumps can be measured for the first time at $z > 0.6$.

Figure 10 is an illustrative example of the unprecedented view that *Chandra* can offer on distant clusters. We show twelve archival images of clusters at $0.7 < z < 1.7$ all covering 2 Mpc (projected at the cluster redshift) and smoothed at the same physical scale (a Gaussian FWHM of 70 kpc). Point-like sources in each field were removed. The intensity (in false colors) is proportional to the square root of the X-ray emission, so that they roughly map the gas density distribution in each cluster. The images are arranged in three redshift bins ($\sim 0.7, 0.8, > 1$), in each row, with X-ray luminosities increasing from left to right. The upper left image shows one of the highest redshift groups known to date, a system discovered in the megasecond exposure of the Chandra Deep Field South (Giacconi et al. 2002) with a core of a few arcseconds. A close inspection of these images reveal a deviation from spherical symmetry in all systems. Some of them are elongated or have cores clearly displaced with respect to the external diffuse envelope (e.g. Holden et al. 2002).

Three of the most luminous clusters at $z \simeq 0.8$ (RXJ1716: Gioia et al. 1999; RXJ0152: Della Ceca et al. 2000, Ebeling et al. 2000a; MS1054: Jeltama et al. 2001) show a double core structure both in the distribution of the gas and in their member galaxies. It is tempting to interpret these morphologies as the result of on-going mergers, although no dynamical information has been gathered to date to support this scenario. In a hierarchical cold dark matter formation scenario, one does expect the most massive clusters at high redshift to be accreting subclumps of comparable masses, and the level of substructure to increase at high redshifts. With current statistical samples however, it is difficult to draw any robust conclusion on the evolution of ICM substructure, which is also found to be a large fraction of the low- z cluster population (e.g. Schücker et al. 2001b).

The third row in Figure 10 show the most distant clusters observed with *Chandra* to date. The first three systems are also among the most distant X-ray selected clusters discovered in the *ROSAT* Deep Cluster Survey (Stanford et al. 2001, 2002), at the very limit of the *ROSAT* sensitivity. RXJ0848 and RXJ0849 are only 5 arcmin apart on the sky (the Lynx field) and are possibly part of a superstructure at $z = 1.26$, consisting of two collapsed, likely virialized clusters (Rosati et al. 1999). Follow-up *Chandra* observations of the Lynx field (Stanford et al. 2001) have yielded for the first time information on ICM morphologies in $z > 1$ clusters and allowed a measurement of their temperatures (see Figure 14 below), implying masses of $(0.5-1) \times 10^{15} h_{50}^{-1} M_{\odot}$. The discovery and the study of these remote systems have the strongest leverage on testing cosmological models.

In Figure 11, we show color composite optical/near-IR images of two clusters at $z > 1$, with overlaid *Chandra* contours. Already at these large lookback times, the temperature and surface brightness profiles of these systems are similar to those of low redshift clusters. Moreover, the morphology of the gas, as traced by the X-ray emission, is well correlated with the spatial distribution of member galaxies, similar to studies at lower redshifts. This suggests that there are already at $z > 1$ galaxy clusters in an advanced dynamical stage of their formation, in which all the baryons (gas and galaxies) have had enough time to thermalize in the cluster potential well. Another example of a $z > 1$ cluster was reported by Hashimoto et al. (2002) using XMM observations of the Lockman Hole.

At $z > 1.3$, X-ray selection has not yielded any cluster based on *ROSAT* data. Follow-up X-ray observations of distant radio galaxies have been used to search for diffuse hot ICM (e.g. Crawford & Fabian 1996). A relatively short *Chandra* observation of the radio galaxy 3C294 at $z = 1.789$ (bottom right in Figure 10)

(Fabian et al. 2001b) has revealed an extended envelope around the central point source, which is the most distant ICM detected so far. Deeper observations are needed to accurately measure the temperature of this system.

5 COSMOLOGY WITH X-RAY CLUSTERS

5.1 The cosmological mass function

The mass distribution of dark matter halos undergoing spherical collapse in the framework of hierarchical clustering is described by the Press-Schechter distribution (PS, Press & Schechter 1974). The number of such halos in the mass range $[M, M + dM]$ can be written as

$$n(M, z)dM = \frac{\bar{\rho}}{M} f(\nu) \frac{d\nu}{dM} dM \quad (10)$$

where $\bar{\rho}$ is the cosmic mean density. The function f depends only on the variable $\nu = \delta_c(z)/\sigma_M$, and is normalized so that $\int f(\nu) d\nu = 1$. $\delta_c(z)$ is the linear-theory overdensity extrapolated to the present time for a uniform spherical fluctuation collapsing at redshift z . This quantity conveys information about the dynamics of fluctuation evolution in a generic Friedmann background. It is convenient to express it as $\delta_c(z) = \delta_0(z) [D(0)/D(z)]$, where $D(z)$ is the linear fluctuation growth factor, which depends on the density parameters contributed by matter, Ω_m and by cosmological constant, Ω_Λ (e.g. Peebles 1993). The quantity $\delta_0(z)$ has a weak dependence on Ω_m and Ω_Λ (e.g. Kitayama & Suto 1997). For a critical-density Universe it is $\delta_0 = 1.686$, independent of z .

The r.m.s. density fluctuation at the mass scale M , σ_M , is connected to the fluctuation power spectrum, $P(k)$, by the relation

$$\sigma_M^2 = \frac{1}{2\pi^2} \int_0^\infty dk k^2 P(k) W^2(kR). \quad (11)$$

The dependence of the power spectrum on the wavenumber k is usually written as $P(k) \propto k^{n_{pr}} T^2(k)$, where $T(k)$ is the transfer function, which depends both on the cosmological parameters of the Friedmann background and on the cosmic matter constituents (e.g. fraction of cold, hot and baryonic matter, number of relativistic species; see Kolb & Turner 1989). For a pure cold dark matter (CDM) model, $T(k)$ depends to a good approximation only on the shape parameter $\Gamma = \Omega_m h$ (e.g. Bardeen et al. 1986), while a correction to this dependence needs to be introduced to account for the presence of the baryonic component (e.g. Eisenstein & Hu 1999). The Harrison-Zel'dovich spectrum is generally assumed with the primordial index, $n_{pr} = 1$, consistent with the most recent analyses of the CMB anisotropies (de Bernardis et al. 2001 and references therein). The amplitude of $P(k)$ is usually expressed in terms of σ_8 , the r.m.s. density fluctuation within a top-hat sphere of $8 h^{-1} \text{Mpc}$ radius. Finally, in Equation 11 $W(x)$ is the Fourier representation of the window function, which describes the shape of the volume from which the collapsing object is accreting matter. The comoving fluctuation size R is connected to the mass scale M as $R = (3M/4\pi\bar{\rho})^{1/3}$ for the top-hat window, i.e. $W(x) = 3(\sin x - x \cos x)/x^3$.

In their original derivation of the cosmological mass function, Press & Schechter (1974) obtained the expression $f(\nu) = (2\pi)^{-1/2} \exp(-\nu^2/2)$ for Gaussian density fluctuations. Despite its subtle simplicity (e.g., Monaco 1998), the PS mass

function has served for more than a decade as a guide to constrain cosmological parameters from the mass function of galaxy clusters. Only with the advent of the last generation of N-body simulations, which are able to span a very large dynamical range, significant deviations of the PS expression from the exact numerical description of gravitational clustering have been noticed (e.g. Gross et al. 1998, Governato et al. 1999, Jenkins et al. 2001, Evrard et al. 2002). Such deviations are interpreted in terms of corrections to the PS approach. For example, incorporating the effects of non-spherical collapse (Sheth et al. 2001) generalizes the above PS expression for $f(\nu)$ to

$$f(\nu) = \sqrt{\frac{2a}{\pi}} C \left(1 + \frac{1}{(a\nu^2)^q} \right) \exp\left(-\frac{a\nu^2}{2}\right), \quad (12)$$

where $a = 0.707$, $C = 0.3222$ and $q = 0.3$ (Sheth & Tormen 1999). The above equation reduces to the PS expression for $a = 1$, $C = 1/2$ and $q = 0$. Fitting formulae for $f(\nu)$, which reproduce N-body results to an accuracy of about 10% (e.g. Evrard et al. 2002) are now currently used to derive cosmological constraints from the evolution of the cluster population.

In practical applications, the observational mass function of clusters is usually determined over about one decade in mass. Therefore, it probes the power spectrum over a relatively narrow dynamical range, and does not provide strong constraints on the shape Γ of the power spectrum. Using only the number density of nearby clusters of a given mass M , one can constrain the amplitude of the density perturbation at the physical scale $R \propto (M/\Omega_m \rho_{crit})^{1/3}$ containing this mass. Since such a scale depends both on M and on Ω_m , the mass function of nearby ($z \lesssim 0.1$) clusters is only able to constrain a relation between σ_8 and Ω_m . In the left panel of Figure 12 we show that, for a fixed value of the observed cluster mass function, the implied value of σ_8 from Equation 12 increases as the density parameter decreases.

Determinations of the cluster mass function in the local Universe using a variety of samples and methods indicate that $\sigma_8 \Omega_m^\alpha = 0.4 - 0.6$, where $\alpha \simeq 0.4 - 0.6$, almost independent of the presence of a cosmological constant term providing spatial flatness (e.g. Bahcall & Cen 1993, Eke et al. 1996, Girardi et al. 1998, Viana & Liddle 1999, Blanchard et al. 2000, Pierpaoli et al. 2001, Reiprich & Böhringer 2002, Seljak 2002, Viana et al. 2002). It is worth pointing out that formal statistical uncertainties in the determination of σ_8 from the different analyses are always far smaller, $\lesssim 5\%$, than the above range of values. This suggests that current discrepancies on σ_8 are likely to be ascribed to systematic effects, such as sample selection and different methods used to infer cluster masses. We comment more on such differences in the following section. Completely independent constraints on a similar combination of σ_8 and Ω_m can be obtained with measurements of the cosmic gravitational lensing shear (e.g. Mellier 1999). The most recent results give $\sigma_8 \Omega_m^{0.6} = 0.45 \pm 0.05$ (van Waerbeke et al. 2001, and references therein).

The growth rate of the density perturbations depends primarily on Ω_m and, to a lesser extent, on Ω_Λ , at least out to $z \sim 1$, where the evolution of the cluster population is currently studied. Therefore, following the evolution of the cluster space density over a large redshift baseline, one can break the degeneracy between σ_8 and Ω_m . This is shown in a pictorial way in Figure 1 and quantified in the right panel of Figure 12: models with different values of Ω_m , which are normalized

to yield the same number density of nearby clusters, predict cumulative mass functions that progressively differ by up to orders of magnitude at increasing redshifts.

5.2 Deriving Ω_m from cluster evolution

An estimate of the cluster mass function is reduced to the measurement of masses for a sample of clusters, stretching over a large redshift range, for which the survey volume is well known.

Velocity dispersions for statistical samples of galaxy clusters have been provided by the ESO Nearby Abell Cluster Survey (ENACS; Mazure et al. 2001) and, more recently, by the 2dF survey (de Propris et al. 2002). Application of this method to a statistically complete sample of distant X-ray selected clusters has been pursued by the CNOC (Canadian Network for Observational Cosmology) collaboration (e.g. Yee et al. 1996). The CNOC sample includes 16 clusters from the EMSS in the redshift range $0.17 \leq z \leq 0.55$. Approximately 100 redshifts of member galaxies were measured for each cluster, thus allowing an accurate analysis of the internal cluster dynamics (Carlberg et al. 1997b). The CNOC sample has been used to constrain Ω_m through the M/L_{opt} method (e.g. Carlberg et al. 1997b), yielding $\Omega_m \simeq 0.2 \pm 0.05$. Attempts to estimate the cluster mass function $n(>M)$ using the cumulative velocity dispersion distribution, $n(>\sigma_v)$, were made (Carlberg et al. 1997b). This method, however, provided only weak constraints on Ω_m owing to the narrow redshift range and the limited number of clusters in the CNOC sample (Borgani et al. 1999, Bahcall et al. 1997). The extension of such methodology to a larger and more distant cluster sample would be extremely demanding from the observational point of view, which explains why it has not been pursued thus far.

A conceptually similar, but observationally quite different method to estimate cluster masses, is based on the measurement of the temperature of the intra-cluster gas (see Section 2). Based on the assumption that gas and dark matter particles share the same dynamics within the cluster potential well, the temperature T and the velocity dispersion σ_v are connected by the relation $k_B T = \beta \mu m_p \sigma_v^2$, where $\beta = 1$ would correspond to the case of a perfectly thermalized gas. If we assume spherical symmetry, hydrostatic equilibrium and isothermality of the gas, the solution of Equation 5 provides the link between the total cluster virial mass, M_{vir} , and the ICM temperature:

$$k_B T = \frac{1.38}{\beta} \left(\frac{M_{vir}}{10^{15} h^{-1} M_\odot} \right)^{2/3} [\Omega_m \Delta_{vir}(z)]^{1/3} (1+z) \text{ keV}. \quad (13)$$

$\Delta_{vir}(z)$ is the ratio between the average density within the virial radius and the mean cosmic density at redshift z ($\Delta_{vir} = 18\pi^2 \simeq 178$ for $\Omega_m = 1$; see Eke et al. 1996 for more general cosmologies). Equation 13 is fairly consistent with hydrodynamical cluster simulations with $0.9 \lesssim \beta \lesssim 1.3$ (e.g. Bryan & Norman 1998, Frenk et al. 2000; see however Voit 2000). Such simulations have also demonstrated that cluster masses can be recovered from gas temperature with a $\sim 20\%$ precision (e.g. Evrard et al. 1996).

Observational data on the $M_{vir}-T$ relation show consistency with the $T \propto M_{vir}^{2/3}$ scaling law, at least for $T \gtrsim 3$ keV clusters (e.g. Allen et al. 2001), but with a $\sim 40\%$ lower normalization. As for lower-temperature systems, Finoguenov et al.

(2001) found some evidence for a steeper slope. Such differences might be due to a lack of physical processes in simulations. For example, energy feedback from supernovae or AGNs and radiative cooling (see Section 2, above) can modify the thermodynamical state of the ICM and the resulting scaling relations.

Measurements of cluster temperatures for flux-limited samples of clusters were made using modified versions of the Piccinotti et al. sample (e.g. Henry & Arnaud 1991). These results have been subsequently refined and extended to larger samples with the advent of *ROSAT*, *Beppo-SAX* and, especially, *ASCA*. With these data one can derive the X-ray Temperature Function (XTF), which is defined analogously to Equation 7. XTFs have been computed for both nearby (e.g. Markevitch 1998, see Pierpaoli et al. 2001, for a recent review) and distant (e.g. Eke et al. 1998, Donahue & Voit 1999, Henry 2000) clusters, and used to constrain cosmological models. The mild evolution of the XTF has been interpreted as a case for a low-density Universe, with $0.2 \lesssim \Omega_m \lesssim 0.6$ (see Figure 13). The starting point in the computation of the XTF is inevitably a flux-limited sample for which $\phi(L_X)$ can be computed. Then the L_X-T_X relation is used to derive a temperature limit from the sample flux limit (e.g. Eke et al. 1998). A limitation of the XTFs presented so far is the limited sample size (with only a few $z \gtrsim 0.5$ measurements), as well as the lack of a homogeneous sample selection for local and distant clusters. By combining samples with different selection criteria one runs the risk of altering the inferred evolutionary pattern of the cluster population. This can give results consistent even with a critical-density Universe (Colafrancesco et al. 1997, Viana & Liddle 1999, Blanchard et al. 2000).

Another method to trace the evolution of the cluster number density is based on the XLF. The advantage of using X-ray luminosity as a tracer of the mass is that L_X is measured for a much larger number of clusters within samples well-defined selection properties. As discussed in Section 3, the most recent flux-limited cluster samples contain now a large (~ 100) number of objects, which are homogeneously identified over a broad redshift baseline, out to $z \simeq 1.3$. This allows nearby and distant clusters to be compared within the same sample, i.e. with a single selection function. The potential disadvantage of this method is that it relies on the relation between L_X and M_{vir} , which is based on additional physical assumptions and hence is more uncertain than the $M_{\text{vir}}-\sigma_v$ or the $M_{\text{vir}}-T$ relations.

A useful parameterization for the relation between temperature and bolometric luminosity is

$$L_{\text{bol}} = L_6 \left(\frac{T_X}{6\text{keV}} \right)^\alpha (1+z)^A \left(\frac{d_L(z)}{d_{L,\text{EdS}}(z)} \right)^2 10^{44} h^{-2} \text{erg s}^{-1}, \quad (14)$$

with $d_L(z)$ the luminosity-distance at redshift z for a given cosmology. Several independent analyses of nearby clusters with $T_X \gtrsim 2$ keV consistently show that $L_6 \simeq 3$ is a stable result and $\alpha \simeq 2.5-3$ (e.g. White et al. 1997, Wu et al. 1999, and references therein). For cooler groups, $\lesssim 1$ keV, the $L_{\text{bol}}-T_X$ relation steepens, with a slope $\alpha \sim 5$ (e.g. Helsdon & Ponman 2000).

The redshift evolution of the L_X-T relation was first studied by Mushotzky & Scharf (1997) who found that data out to $z \simeq 0.4$ are consistent with no evolution for an Einstein-de-Sitter model (i.e., $A \simeq 0$). This result was extended to higher redshifts using cluster temperatures out to $z \simeq 0.8$ as measured with

ASCA and *Beppo-SAX* data (Donahue et al. 1999, Della Ceca et al. 2000, Henry 2000). The lack of a significant evolution seems to hold beyond $z = 1$ according to recent *Chandra* observations of very distant clusters (Borgani et al. 2001b, Stanford et al. 2001, Holden et al. 2002), as well as *Newton-XMM* observations in the Lockman Hole (Hashimoto et al. 2002). Figure 14 shows a summary of the observational results on the L_X - T . The high redshift points generally lie around the local relation, thus demonstrating that it is reasonable to assume $A \lesssim 1$ implying at most a mild positive evolution of the L_{bol} - T_X relation. Besides the relevance for the evolution of the mass-luminosity relation, these results also have profound implications for the physics of the ICM (see Section 2).

Kitayama & Suto (1997) and Mathiesen & Evrard (1998) analyzed the number counts from different X-ray flux-limited cluster surveys (Figure 7) and found that resulting constraints on Ω_m are rather sensitive to the evolution of the mass-luminosity relation. Sadat et al. (1998) and Reichart et al. (1999) analyzed the EMSS and found results to be consistent with $\Omega_m = 1$. Borgani et al. (2001b) analyzed the RDCS sample to quantify the systematics in the determination of cosmological parameters induced by the uncertainty in the mass-luminosity relation (Borgani et al. 1998). They found $0.1 \lesssim \Omega_m \lesssim 0.6$ at the 3σ confidence level, by allowing the M - L_X relation to change within both the observational and the theoretical uncertainties. In Figure 15 we show the effect of changing in different ways the parameters defining the M - L_X relation, such as the slope α and the evolution A of the L_X - T relation (see Equation 14), the normalization β of the M - T relation (see Equation 13), and the overall scatter Δ_{M-L_X} . We assume flat geometry here, i.e. $\Omega_m + \Omega_\Lambda = 1$. In general, constraints of cosmological models based on cluster abundance are not very sensitive to Ω_Λ (see Figure 12). To a first approximation, the best fit Ω_m has a slight dependence on Ω_Λ for open geometry: $\Omega_m \simeq \Omega_{m,fl} + 0.1(1 - \Omega_{m,fl} - \Omega_\Lambda)$, where $\Omega_{m,fl}$ is the best fit value for flat geometry.

Constraints on Ω_m from the evolution of the cluster population, like those shown in Figures 13 and 15, are in line with the completely independent constraints derived from the baryon fraction in clusters, f_{bar} , which can be measured with X-ray observations. If the baryon density parameter, Ω_{bar} , is known from independent considerations (e.g. by combining the observed deuterium abundance in high-redshift absorption systems with predictions from primordial nucleosynthesis), then the cosmic density parameter can be estimated as $\Omega_m = \Omega_{bar}/f_{bar}$ (e.g. White et al. 1993b). For a value of the Hubble parameter $h \simeq 0.7$, this method yields $f_{bar} \simeq 0.15$ (e.g. Evrard 1997; Ettori 2001). Values of f_{bar} in this range are consistent with $\Omega_m = 0.3$ for the currently most favored values of the baryon density parameter, $\Omega_{bar} \simeq 0.02 h^{-2}$, as implied by primordial nucleosynthesis (e.g. Burles & Tytler 1998) and by the spectrum of CMB anisotropies (e.g. de Bernardis et al. 2001, Stompor et al. 2001, Pryke et al. 2002).

Figure 15 demonstrates that firm conclusions about the value of the matter density parameter Ω_m can be drawn from available samples of X-ray clusters. In keeping with most of the analyses in the literature, based on independent methods, a critical density model cannot be reconciled with data. Specifically, $\Omega_m < 0.5$ at 3σ level even within the full range of current uncertainties in the relation between mass and X-ray luminosity.

A more delicate issue is whether one can use the evolution of galaxy clusters for high-precision cosmology, e.g., $\lesssim 10\%$ accuracy. Serendipitous searches of distant clusters from XMM and Chandra data will eventually lead to a significant

increase of the number of high- z clusters with measured temperatures. Thus, the main limitation will lie in systematics involved in comparing the mass inferred from observations with that given by theoretical models. A point of concern, for example, is that constraints on σ_8 from different analyses of the cluster abundance differ by up to 30% from each other. While a number of previous studies found $\sigma_8 \simeq 0.9$ –1 for $\Omega_m = 0.3$ (e.g. Pierpaoli et al. 2001 and references therein), the most recent analyses point toward a low power spectrum normalization, $\sigma_8 \simeq 0.7$ for $\Omega_m = 0.3$ (Borgani et al. 2001b, Reiprich & Böhringer 2002, Seljak 2002, Viana et al. 2002).

A thorough discussion of the reasons for such differences would require an extensive and fairly technical review of the analysis methods applied so far. For instance, a delicate point concerns the different recipes adopted for the mass–temperature and mass–luminosity conversions. The M – T relation, usually measured at some fixed overdensity from observational data, seems to have a lower normalization than that calibrated from hydrodynamical simulations (e.g. Finoguenov et al. 2001, Allen et al. 2001, Ettori et al. 2002). In turn, this provides a lower amplitude for the mass function implied by an observed XTF and, therefore, a smaller σ_8 . Several uncertainties also affect the L_X – T relation. The derived slope depends on the temperature range over which the fit is performed. We are also far from understanding the nature of its scatter, i.e. how much it is due to systematics, and how much it is intrinsic, inherent to complex physical conditions in the gas. For example, the contribution of cooling flows is known to increase the scatter in the L_X – T relation (e.g. Markevitch 1998, Allen & Fabian 1998, Arnaud & Evrard 1999). Adding such a scatter in the mass–luminosity conversion increases the amplitude of the mass–function, especially in the high-mass tail, thus decreasing the required σ_8 .

As an illustrative example, we show in Figure 15 how constraints in the σ_8 – Ω_m plane move as we change the scatter and the amplitude of the M – L_X relation in the analysis of the RDCS. The upper left panel shows the result for the same choice of parameters as in the original analysis by Borgani et al. (2001b), which gives $\sigma_8 \simeq 0.7$ for $\Omega_m = 0.3$. The central lower panel shows the effect of decreasing the scatter of the M – L_X relation by 20%, in keeping with the analysis by Reiprich & Böhringer (2002, see also Ettori et al. 2002). Such a reduced scatter causes σ_8 to increase by about 20%. Finally, if the normalization of the M – T relation is decreased by $\sim 30\%$ with respect to the value suggested by hydrodynamical cluster simulations (lower right panel), σ_8 is again decreased by $\sim 20\%$.

In light of this discussion, a 10% precision in the determination of fundamental cosmological parameters, such as Ω_m and σ_8 lies in the future. With forthcoming datasets the challenge will be in comparing observed clusters with the theoretical clusters predicted by Press-Schechter–like analytical approaches or generated by numerical simulations of cosmic structure formation.

6 OUTLOOK AND FUTURE WORK

Considerable observational progress has been made in tracing the evolution of global physical properties of galaxy clusters as revealed by X-ray observations. The *ROSAT* satellite has significantly contributed to providing the statistical samples necessary to compute the space density of clusters in the local Universe and its evolution. A great deal of optical spectroscopic studies of these samples

has consolidated the evidence that the bulk of the cluster population has not evolved significantly since $z \sim 1$. However, the most X-ray luminous, massive systems do evolve. Similarly, the thermodynamical properties of clusters as indicated by statistical correlations, such as the $L_X - T_X$ relation, do not show any strong evolution. Moreover, the *Chandra* satellite has given us the first view of the gas distribution in clusters at $z > 1$; their X-ray morphologies and temperatures show that they are already in an advanced stage of formation at these large lookback times.

These observations can be understood in the framework of hierarchical formation of cosmic structures, with a low density parameter, $\Omega_m \sim 1/3$, dominated by cold dark matter: structure formation started at early cosmic epochs and a sizable population of massive clusters was in place already at redshifts of unity. In addition, detailed X-ray observation of the intra-cluster gas show that the physics of the ICM needs to be regulated by additional non-gravitational processes.

With *Chandra* and *Newton-XMM*, we now realize that physical processes in the ICM are rather complex. Our physical models and numerical simulations are challenged to explain the new level of spatial details in the density and temperature distribution of the gas, and the interplay between heating and cooling mechanisms. Such complexities need to be well understood physically before we can use clusters as high-precision cosmological tools, particularly at the beginning of an era in which cosmological parameters can be derived rather accurately by combining methods that measure the global geometry of the Universe (the CMB spectrum, type Ia Supernovae (e.g. Leibungut 2001)), and the large-scale distribution of galaxies (e.g. Peacock et al. 2001). It remains remarkable that the evolution of the cluster abundance, the CMB fluctuations, the type Ia Supernovae and large scale structure – all completely independent methods – converge toward $\Omega_m \simeq 0.3$ in a spatially flat Universe ($\Omega_m + \Omega_\Lambda = 1$). Further studies with the current new X-ray facilities will help considerably in addressing the issue of systematics discussed above, although some details of the ICM in $z \gtrsim 1$ clusters, such as temperature profiles or metallicity, will remain out of reach until the next generation of X-ray telescopes. Direct measurements of cluster masses at $z \gtrsim 1$ via gravitational lensing techniques will soon be possible with the *Advanced Camera for Surveys* (Ford et al. 1998) on-board the *Hubble Space Telescope*, which offers an unprecedented combination of sensitivity, angular resolution and field of view.

The fundamental question remains as to the mode and epoch of formation of the ICM. When and how was the gas pre-heated and polluted with metals? What is the epoch when the first X-ray clusters formed, i.e. the epoch when the accreted gas thermalizes to the point at which they would lie on the $L_X - T$ relation (Figure 14)? Are the prominent concentrations of star forming galaxies discovered at redshift $z \sim 3$ (Steidel et al. 1998) the progenitors of the X-ray clusters we observed at $z \lesssim 1$? If so, cluster formation should have occurred in the redshift range 1.5–2.5. Although the redshift boundary for X-ray clusters has receded from $z = 0.8$ to $z = 1.3$ recently, a census of clusters at $z \simeq 1$ has just begun and the search for clusters at $z > 1.3$ remains a serious observational challenge. Using high- z radio galaxies as signposts for proto-clusters has been the only viable method so far to break this redshift barrier. These searches have also lead to the discovery of extended $Ly\alpha$ nebulae around distant radio galaxies (e.g., Venemans et al. 2002), very similar to those discovered by Steidel et al. (2000) in correspondence with large scale structures at $z \simeq 3$. The nature of

such nebulae is still not completely understood, however they could represent the early phase of collapse of cool gas through mergers and cooling flows.

In this review we have not treated the formation and evolution of the galaxies in clusters. This must be linked to the evolution of the ICM and the fact that we are still treating the two aspects as separate points to the difficulty in drawing a comprehensive unified picture of the history of cosmic baryons in their cold and hot phase. Multiwavelength studies are undoubtedly essential to reach such a unified picture. When surveys exploiting the Sunyaev–Zeldovich effect (e.g. Carlstrom et al. 2001) over large solid angles become available, one will be able to observe very large volumes at $z > 1$. In combination with a deep large area X-ray survey (e.g. Wide Field X-ray Telescope, Burrows et al. 1992) and an equivalent deep near-IR survey (e.g. the Primordial Explorer (PRIME), Zheng et al. 2002), this could reveal the evolutionary trends in a number of independent physical parameters, including: the cluster mass, the gas density and temperature, the underlying galactic mass and star formation rates. Advances in instrumentation and observational technique will make this approach possible and will provide vital input for models of structure formation and tight constraints on the underlying cosmological parameters.

ACKNOWLEDGMENTS

We acknowledge useful discussions with Hans Böhringer, Alfonso Cavaliere, Guido Chincarini, Roberto Della Ceca, Stefano Ettori, Gus Evrard, Isabella Gioia, Luigi Guzzo, Brad Holden, Silvano Molendi, Chris Mullis, and Adam Stanford. We thank Paolo Tozzi for his help in producing Figure 10. PR thanks Riccardo Giacconi for continuous encouragement of this work. PR is grateful for the hospitality of the Astronomical Observatory of Trieste. SB and CN acknowledge the hospitality and support of ESO in Garching.

Literature Cited

1. Abell GO. 1958. *Ap. J. Suppl.* 3:211–278.
2. Abell GO, Corwin HGJr, Olowin RP. 1989. *Ap. J. Suppl.* 70:1–138
3. Allen SW, Fabian AC. 1998. *MNRAS* 297:L57–62
4. Allen SW, Schmidt RW, Fabian AC. 2001. *MNRAS* 328:L37–41
5. Allen SW, Schmidt RW, Fabian AC. 2002. *MNRAS* in press. Preprint astro-ph/0111368
6. Arnaud M, Evrard CE. 1999. *MNRAS* 305:631–640
7. Bahcall NA. 1988. *Annu. Rev. Astron. Astrophys.* 26:631–686
8. Bahcall NA, Cen R. 1993. *Ap. J. Lett.* 407:L49–52
9. Bahcall NA, Fan X, Cen R. 1997. *Ap. J. Lett.* 485:L53–56
10. Bahcall NA, Ostriker JP, Perlmutter S, Steinhardt PJ. 2000. *Science*, 284:1481–88
11. Balogh ML, Babul A, Patton DR. 1999. *MNRAS* 307:463–479
12. Balogh, ML, Pearce FR, Bower RG, Kay ST 2001. *MNRAS* 326:1228–1234
13. Bardeen JM, Bond JR, Kaiser N, Szalay AS. 1986. *Ap. J.* 304:15–61
14. Bauer FE, Alexander DM, Brandt WN, Hornschemeier AE, Miyaji T, Garmire DP. 2002. *Astron. J.* 123:1163–1178
15. Benítez N, Broadhurst T, Rosati P, Courbin F, Squires G, Lidman C, Magain P. 1999. *Ap. J.* 527:31–41
16. de Bernardis P, Ade PAR, Bock JJ, Bond JR, Borrill J. 2001. *Ap. J.* 561:13–21
17. Bialek JJ, Evrard AE, Mohr JJ. 2001. *Ap. J.* 555:597–612
18. Birkinshaw M. 1999. *Phys. Rep.* 310:97–195
19. Blanchard A, Sadat R, Bartlett JG, Le Dour M. 2000. *Astron. Astrophys.* 362:809–824
20. Blanton MR, Dalcanton J, Eisenstein D, Loveday J, Strauss MA, et al. 2001. *Astron. J.* 121:2358–2380

21. Böhringer H, Voges W, Huchra JP, McLean B, Giacconi R, et al. 2000. *Ap. J. Suppl.* 129:435–474
22. Böhringer H, Schuecker P, Guzzo L, Collins CA, Voges W, et al. 2001. *Astron. Astrophys.* 369:826–50
23. Böhringer H, Matsushita K, Churazov E, Ikebe Y, Chen Y. 2002a. *Astron. Astrophys.* 382:804–20
24. Böhringer H, Collins CA, Guzzo L, Schuecker P, Voges W, et al. 2002b. *Ap. J.* 566:93–102
25. Borgani S, Girardi M, Carlberg RG, Yee HKC, Ellingson E. 1999. *Ap. J.* 527: 561–572
26. Borgani S, Guzzo L. 2001. *Nature* 409:39–45
27. Borgani S, Rosati P, Tozzi P, Norman C. 1998. *Ap. J.* 517:40–53
28. Borgani S, Governato F, Wadsley J, Menci N, Tozzi P., et al. 2001a, *Ap. J. Lett.* 559:L71–74
29. Borgani S, Rosati P, Tozzi P, Stanford, Eisenhardt PE, et al. 2001b. *Ap. J.* 561:13–21
30. Bower RG, Benson AJ, Bough CL, Cole S, Frenk CS, Lacey CG. 2001. *MNRAS.* 325:497–508
31. Brighenti F, Mathews WG. 2001. *ApJ* 553:103–120
32. Bryan GL 2000. *Ap. J. Lett.* 544:L1–L4
33. Bryan GK, Norman ML. 1998. *Ap. J.* 495:80–99
34. Burns JO, Ledlow MJ, Loken C, Klypin A, Voges W, et al. 1996. *Ap. J. Lett.* 467:L49–52
35. Burke DJ, Collins CA, Sharples RM, Romer AK, Holden, BP, Nichol, RC, et al. 1997. *Ap. J. Lett.* 488:L83–86
36. Burles S, Tytler D. 1998. *Space Sc. Rev.* 84(1/2):65–75
37. Burns JO, Ledlow MJ, Loken C, Klypin A, Voges W., et al. 1996. *Ap. J. Lett.* 467:L49–52
38. Burrows CJ, Burg R, Giacconi R. 1992. *Ap. J.* 392:760–765
39. Campana S, Lazzati D, Panzera MR, Tagliaferri G. 1999. *Ap. J.* 524:423–433
40. Carlberg RG, Yee HKC, Ellingson E. 1997a. *Ap. J.* 478:462–475
41. Carlberg RG, Morris SL, Yee HKC, Ellingson E, 1997b. *Ap. J. Lett.* 479:L19–23
42. Carlstrom JE, Joy M, Grego L, Holder G, Holzappel WL, et al. 2001. In *Constructing the Universe with Clusters of Galaxies*, eds. F. Durret and G. Gerbal. Preprint astro-ph/0103480
43. Carroll SM, Press WH, Turner EL. 1992. *Annu. Rev. Astron. Astrophys.* 30:499–542
44. Castander FJ, Bower RG, Ellis RS, Aragon-Salamanca A, Mason KO, et al. 1995. *Nature* 377:39–41
45. Cavaliere A, Fusco-Femiano R. 1976. *Astron. Astrophys.* 49:137–144
46. Cavaliere A, Gursky H, Tucker WH. 1971. *Nature* 231:437–438
47. Cavaliere A, Menci N, Tozzi P. 1998. *Ap. J.* 501:493–508
48. Chartas G, Bautz M, Garmire G, Jones C, Schneider DP. 2001. *Ap. J. Lett.* 550:L163–166
49. Colafrancesco S, Mazzotta P, Vittorio N. 1997. *ApJ* 488:566–571
50. Coles P, Lucchin F. 1995. *Cosmology. The origin and evolution of cosmic structure*, Chichester, Wiley
51. Collins CA, Burke DJ, Romer AK, Sharples RM, Nichol RC. 1997. *Ap. J. Lett.* 479:L117–120
52. Collins CA, Guzzo L, Böhringer H, Schücker P, Chincarini G, et al. 2000. *MNRAS* 319:939–948
53. Couch WJ, Ellis RS, MacLaren I, Malin DF. 1991. *MNRAS* 249: 606–628
54. Crawford CS, Edge AC, Fabian AC, Allen SW, Böhringer H, et al. 1995. *MNRAS* 274:75–84
55. Crawford CS, Fabian AC. 1996. *MNRAS* 282:1483–1488
56. Dalcanton JJ. 1996. *Ap. J.* 466:92–103
57. Dalton GB, Maddox SJ, Sutherland WJ, Efstathiou G. 1997. *MNRAS* 289:263–284
58. De Grandi S, Böhringer H, Guzzo L, Molendi S, Chincarini G, et al. 1999. *Ap. J.* 514:148–163
59. De Grandi S, Molendi S. 2001 *Ap. J.* 551:153–159
60. De Grandi S, Molendi S. 2002 *Ap. J.* 567:163–177
61. Della Ceca R, Scaramella R, Gioia IM, Rosati P, Fiore F, Squires G. 2000. *Astron. Astrophys.* 353:498–506
62. de Propris R, the 2dFGRS team 2002. *MNRAS* 329:87–101
63. Dickinson M, 1997, in *The Early Universe with the VLT*, ed. J. Bergeron, (Springer: Berlin) p.274
64. Donahue M, Voit GM, Scharf CA, Gioia IM, Mullis CR, et al. 1999. *Ap. J.* 527:525–534
65. Donahue M, Voit GM. 1999. *Ap. J. Lett.* 523:L137–140
66. Donahue M, Mack J, Scharf C, Lee P, Postman M, et al. 2001. *Ap. J. Lett.* 552:L93–96
67. Ebeling H, Voges W, Böhringer H, Edge AC, Huchra JP, Briel UG. 1996. *MNRAS* 281:799–829
68. Ebeling H, Edge AC, Fabian AC, Allen SW, Crawford CS, Böhringer H. 1997. *Ap. J. Lett.*

- 479:L101–104
69. Ebeling H, Edge AC, Bohringer H, Allen SW, Crawford CS, et al. 1998. *MNRAS* 301:881–914
 70. Ebeling H, Jones LR, Perlman E, Scharf C, Horner D, et al. 2000. *Ap. J.* 534:133–145
 71. Ebeling H, Edge AC, Allen SW, Crawford CS, Fabian AC, Huchra JP. 2000, *MNRAS* 318:333–340
 72. Ebeling A, Edge AC, Henry JP. 2001. *Ap. J.* 553:668–676
 73. Edge AC, Stewart GC, Fabian AC, Arnaud KA, 1990. *MNRAS* 245:559–569
 74. Eke VR, Cole S, Frenk CS. 1996. *MNRAS* 282:263–280
 75. Eke VR, Cole S, Frenk CS, Henry JP. 1998. *MNRAS*, 298:1145–1158
 76. Eisenstein DJ, Hu W. 1999. *Ap. J.* 511:5–15
 77. Ettori S. 2001. *MNRAS* 323:L1–L5
 78. Ettori S, De Grandi S, Molendi S. 2002. *Astron. Astrophys.* in press. Preprint astro-ph/0206120
 79. Evrard AE. 1997. *MNRAS* 292:289–297
 80. Evrard AE, Henry JP. 1991. *Ap. J.* 383:95–103
 81. Evrard, AE, MacFarland TJ, Couchman HMP, Colberg JM, Yoshida N, et al. 2002. *Ap. J.* 573:7–36
 82. Evrard AE, Metzler CR, Navarro JF. 1996. *Ap. J.* 469:494–507
 83. Fabian AC. 1994. *Annu. Rev. Astron. Astrophys.* 32:277–318
 84. Fabian AC, Sanders JS, Ettori S, Taylor GB, Allen SW, et al. 2000. *MNRAS* 318:L65–68
 85. Fabian AC, Mushotzky RF, Nulsen PEJ, Peterson JR. 2001. *MNRAS* 321:L20–L24
 86. Fabian AC, Crawford CS, Ettori S, Sanders JS. 2001. *MNRAS* 332:L11–L15
 87. Felten JE, Gould RJ, Stein WA, Woolf NJ. 1966. *Ap. J.* 146:955–958
 88. Finoguenov A, David LP, Ponman TJ. 2000. *Ap. J.* 544:188–203
 89. Finoguenov A, Reiprich TH, Böhringer H. 2001. *Astron. Astrophys.* 368:749–759
 90. Ford HC and the ACS Science Team. 1998. In *Space Telescopes and Instruments V*, eds. PY Bely, JB Breckinridge, Proc. SPIE, 3356, 234.
 91. Forman W, Jones C. 1982. *Annu. Rev. Astron. Astrophys.* 20:547–585
 92. Francis PJ, Woodgate BE, Warren SJ, Moller P, Mazzolini M, et al. 1996. *Ap. J.* 457:490–499
 93. Frenk CS, White SDM, Bode P, Bond JR, Bryan GL, et al. 2000. *ApJ* 525:554–582
 94. Giacconi R, Murray S, Gursky H, Kellogg E, Schreier E, Tananbaum H. 1972. *Ap. J.* 178:281–308
 95. Giacconi R, Branduardi G, Briel U, Epstein A, Fabricant D, et al. 1979. *Ap. J.* 230:540–550
 96. Giacconi R, Zirm A, JunXian W, Rosati P, Nonino M, et al. 2002. *Ap. J. Suppl.* 139:369–410
 97. Gioia IM, Henry JP, Maccacaro T, Morris SL, Stocke JT, Wolter A. 1990a. *Ap. J. Lett.* 356:L35–38
 98. Gioia IM, Maccacaro T, Schild RE, Wolter A, Stocke JT, et al. 1990b. *Ap. J. Suppl.* 72:567–619
 99. Gioia IM, Luppino GA. 1994. *Ap. J. Suppl.* 94:583–614
 100. Gioia IM, Henry JP, Mullis CR, Ebeling H, Wolter A. 1999. *Astron. J.* 117:2608–2616
 101. Gioia IM, Henry JP, Mullis CR, Voges W, Briel UG. 2001. *Ap. J. Lett.* 553:L109–112
 102. Girardi M, Borgani S, Giuricin G, Mardirossian F, Mezzetti M. 1998. *Ap. J.* 506:45–52
 103. Girardi M, Mezzetti M. 2001. *Ap. J.* 540:79–96
 104. Gladders MD, Yee HKC. 2000. *Astron. J.* 120:2148–2162
 105. Gonzales AH, Zaritsky D, Dalcanton JJ, Nelson A. 2001. *Ap. J. Suppl.* 137:117–138
 106. Governato F, Babul A, Quinn T, Tozzi P, Baugh CM, et al. 1999. *MNRAS* 307:949–966
 107. Gursky H, Kellogg E, Murray S, Leong C, Tananbaum H, Giacconi, R. 1971. *Ap. J.* 167:L81–84
 108. Gross MAK, Somerville RS, Primack JR, Holtzman J, Klypin, A. 1998. *MNRAS* 301:81–94
 109. Gunn JE, Hoessel JG, Oke JB. 1986. *Ap. J.* 306:30–37
 110. Hashimoto Y, Hasinger G, Arnaud M, Rosati P, Miyaji T. 2002. *Astron. Astrophys.* 381:841–847
 111. Hattori M, Matuzawa H, Morikawa K, Kneib J-P, Yamashita K, et al. 1998. *Ap. J.* 503:593–598
 112. Hall PB, Green RF. 1998. *Ap. J.* 558:558–584
 113. Hasinger G, Altieri B, Arnaud M, Barcons X, Bergeron J, et al. 2001. *Astron. Astrophys.* 365:L45–L50
 114. Helsdon SF, Ponman TJ. 2000. *MNRAS* 315:356–370

115. Henriksen MJ, Mushotzky RF. 1986. *Ap J.* 302:287–295
116. Henry JP. 2000. *Ap. J.* 534:565–580
117. Henry JP, Arnaud KA. 1991. *Ap. J.* 372:410–418
118. Henry JP, Gioia IM, Maccacaro T, Morris SL, Stocke JT, Wolter A. 1992. *Ap. J.* 386:408–419
119. Henry JP, Gioia IM, Mullis CR, Voges W, Briel UG, et al. 2001. *Ap. J. Lett.* 553:L109–112
120. Holden BP, Nichol RC, Romer AK, Metevier A, Postman M, et al. 1999. *Astron. J.* 118:2002–2013
121. Holden B, Stanford SA, Squires GK, Rosati P, Tozzi P, et al. 2002. *Astron. J.*, 124:35–45
122. Kaiser N. 1986. *MNRAS* 222:323–345
123. Kellogg E, Gursky H, Leong C, Schreier E, Tananbaum H, Giacconi R. 1971. *Ap. J.* 165:L49–54
124. Kim RSJ, Kepner JV, Postman M, Strauss MA, Bahcall NA, et al. 2002. *Astron. J.* 123:20–36
125. Kitayama T, Suto Y. 1997. *Ap. J.* 490:557–563
126. Kofman LA, Gnedin NJ, Bahcall NA. 1993. *Ap. J.* 413:1–19
127. Kolb KT, Turner MS. 1989. *The Early Universe* Addison–Wesley Publ.
128. Kravtsov AV, Yepes G. 2000. *MNRAS* 318:227–238
129. Irwin JA, Bregman JN. 2000. *Ap. J.* 538:543–554
130. Jeltama TE, Canizares CR, Bautz MW, Malm MR, Donahue M, Garmire GP. 2001. *Ap. J.* 562:124–132
131. Jenkins A, Frenk CS, White SDM, Colberg J, Cole S, et al. 2001. *MNRAS* 321:372–384
132. Jones LR, Scharf C, Ebeling H, Perlman E, Wegner G, et al. 1998. *Ap. J.*, 495:100–114
133. Jones LR, Ebeling H, Scharf C, Perlman E, Horner D, et al. 2000. in *Constructing the Universe with clusters of Galaxies*, eds Durret F & Gerbal D (CD-rom, website)
134. Kristian J, Sandage A, Westphal JA. 1978, *Ap. J.* 221:383–394
135. Lazzati D, Campana S, Rosati P, Panzera MR, Tagliaferri G. 1999. *Ap. J.* 524:414–422
136. Leibungut B. 2002. *Annu. Rev. Astron. Astrophys.* 39:67–98
137. Lewis AD, Ellingson E, Morris SL, Carlberg RG. 1999. *Ap. J.* 517:587–608
138. Lidman EL, Peterson BA. 1996. *Ap. J* 112:2454–2470
139. Lloyd-Davies EJ, Ponman TJ, Cannon DB. 2000. *MNRAS* 315:689–702
140. Lubin LM, Brunner R, Metzger MR, Postman M, Oke JB. 2000. *Ap. J.* 531:L5–8
141. Lumsden SL, Nichol RC, Collins CA, Guzzo L. 1992. *MNRAS* 258:1–22
142. Maddox SJ, Efstathiou G, Sutherland WJ, Loveday J. 1990. *MNRAS* 242:43p–47p
143. Markevitch M. 1998. *Ap. J.* 504:27–34
144. Markevitch M, Forman WR, Sarazin CL, Vikhlinin A. 1998. *Ap. J.* 503:77–96
145. Markevitch M, Ponman TJ, Nulsen PEJ, Bautz MW, Burke DJ, et al. 2000. *Ap. J.* 541:542–549
146. Mathiesen B, Evrard AE. 1998. *MNRAS* 295:769–780
147. Mazure A, Katgert P, den Hartog R, Biviano A, Dubath P., et al. 2001. *Astron. Astrophys.* **310**:31–48
148. McHardy IM, Lawrence A, Pye JP, Pounds KA. 1981. *Ap. J.* 197:893–919
149. McKee JD, Mushotzky RF, Boldt EA, Holt SS, Marshall FE, et al. 1980. *Ap. J.* 242:843–856
150. Mellier Y. 1999. *Annu. Rev. Astron. Astrophys.* 37:127–189
151. Menci N, Cavaliere A. 2000. *MNRAS* 311:50–62
152. Monaco P. 1998. *Fund. Cosm. Phys.* 19:157–317
153. Muanwong O, Thomas PA, Kay ST, Pearce FR, Couchman HMP. 2001. *Ap. J.* 552:L27–30
154. Mulchaey JS. 2000. *Annu. Rev. Astron. Astrophys.* 38:289–335
155. Mullis CR, Henry JP, Gioia IM, Böhringer H, Briel UG, et al. 2001. *Ap. J. Lett.* 553:L115–118
156. Mushotzky RF, Scharf CA. 1997. *Ap. J. Lett.* 482:L13–16
157. Navarro JF, Frenk CS, White SDM. 1995. *MNRAS* 275:720–740
158. Nichol RC, Romer AK, Holden BP, Ulmer MP, Pildis RA, et al. 1999 *Ap. J.* 521:L21–L24
159. Olsen LF, Scodreggio M, da Costa LN, Slijkhuis R, Benoist C, et al. 1999. *Astron. Astrophys.* 345:363–368
160. Oukbir J, Blanchard A 1992. *Astron. Astrophys.* 262:L21–24
161. Page MJ, Carrera FJ. 2000. *MNRAS* 311:433–440
162. Pascarelle SM, Windhorst RA, Drivers SP, Ostrander EJ, Keel WC. 1996. *Ap. J. Lett.*

- 456:L21–24
163. Pearce FR, Thomas PA, Couchman HMP, Edge AC. 2000. *MNRAS* 317:1029–1040
 164. Peacock JA. 1999. *Cosmological Physics*, Cambridge University Press, Cambridge
 165. Peacock JA, Cole S, Norberg P, Baugh CM, Bland–Hawthorn J, et al. 2001. *Nature* 412:169–173
 166. Peebles PJE. 1993. *Physical Cosmology* Princeton, NJ: Princeton Univ. Press
 167. Pentericci L, Kurk JD, Röttgering HJA, Miley GK, van Breugel W, et al. 2000. *Astron. Astrophys.* 361:L25–28
 168. Perlman ES, Horner DJ, Jones LR, Scharf CA, Ebeling H, et al. 2002 *Ap. J. Suppl.* 140:265–301
 169. Peterson JR, Paerels FBS, Kaastra JS, Arnaud M, Reiprich TH, et al. 2001. *Astron. Astrophys.* 365:L104–L109
 170. Piccinotti G, Mushotzky RF, Boldt EA, Holt SS, Marshall FE, et al. 1982. *Ap. J.* 253:485–503
 171. Pierpaoli E, Scott D, White M. 2001. *MNRAS* 325:77–88
 172. Pipino A, Matteucci F, Borgani S, Biviano A. 2002. *New Astron.* 7:227–247
 173. Ponman TJ, Cannon DB, Navarro JF. 1999. *Nature* 397:135–137
 174. Postman M, Lubin LM, Gunn JE, Oke JB, Hoessel JG, Schneider DP, Christensen JA. 1996. *Astron. J.* 111:615–641
 175. Press WH, Schechter P. 1974. *Ap. J.* 187:425–438
 176. Pryke C, Halverson NW, Leitch EM, Kovac J, Carlstrom JE, et al. 2002 *Ap. J.* 568:46–51
 177. Raymond JC, Smith BW. 1977. *Ap. J. Suppl.* 35:419–439
 178. Reichart DE, Nichol RC, Castander FJ, Burke DJ, Romer AK, et al. 1999. *Ap. J.* 518:521–532
 179. Reiprich TH, Böhringer H. 2002 *Ap. J.* 567:716–740
 180. Renzini A. 1997. *Ap. J.* 488:35–43
 181. Romer AK, Nichol RC, Holden BP, Ulmer MP, Pildis RA, et al. 2000. *Ap. J. Suppl.*, 126:209–269
 182. Rosati P, Borgani S, Della Ceca R, Stanford SA, Eisenhardt PR, Lidman C. 2000. In *Large Scale Structure in the X-ray Universe*, ed M Plionis, I Georgantopoulos, p.13. Paris, France: Atlantisciences
 183. Rosati P, Della Ceca R, Burg R, Norman C, Giacconi R. 1995. *Ap. J. Lett.* 445:L11–14
 184. Rosati P, Della Ceca R, Burg R, Norman C, Giacconi R. 1998. *Ap. J. Lett.* 492:L21–24
 185. Rosati P, Stanford SA, Eisenhardt PR, Elston R, Spinrad H, et al. 1999. *Astron. J.* 118:76–85
 186. Rothschild R. et al. 1979 *Space Sci. Instr.* 4:265
 187. Sadat R, Blanchard A, Oukbir J. 1998. *Astron. Astrophys.* 329:21–29
 188. Sarazin C. 1988. *X-Ray Emission from Clusters of Galaxies*. Cambridge: Cambridge University Press
 189. Scharf CA, Jones LR, Ebeling H, Perlman E, Malkan M, et al. 1997. *Ap. J.* 477:79–92
 190. Schücker P, Böhringer H, Guzzo L, Collins CA, Neumann DM, et al. 2001. *Astron. Astrophys.* 368:86–106
 191. Schücker P, Böhringer H, Reiprich TH, Feretti L. 2001. *Astron. Astrophys.* 378:408–427
 192. Seljak U. 2002. *MNRAS* submitted. Preprint astro-ph/0111362
 193. Sheth RK, Tormen G. 1999. *MNRAS* 308:119–126
 194. Sheth RK, Mo HJ, Tormen G. 2001. *MNRAS* 323:1–12
 195. Smith S. 1936. *Ap. J.* 83:23–30
 196. Stanford SA, Elston R, Eisenhardt PR, Spinrad H, Stern D, Dey A. 1997. *Astron. J.* 114:2232–2239
 197. Stanford SA, Holden B, Rosati P, Tozzi P, Borgani S, et al. 2001. *Ap. J.* 552:504–507
 198. Stanford SA, Holden BP, Rosati P, Eisenhardt PR, Stern D, et al. 2002. *Astron. J.* 123:619–626
 199. Steidel CC, Adelberger KL, Dickinson M, Giavalisco M, Pettini M, Kellogg M. 1998. *Ap. J.* 492:428–438
 200. Steidel CC, Adelberger KL, Shapley AE, Pettini M, Dickinson M, Giavalisco M. 2000. *Ap. J.* 532:170–182
 201. Stompor S, Abroe M, Ade P, Balbi A, Barbosa D, et al. 2001. *Ap. J. Lett.* 561:L7–10
 202. Soucail G, Kneib J-P, Jaunsen AO, Hjorth J, Hattori M, Yamada T. 2001. *Astron. Astrophys.* 367:741–747

203. Tamura T, Kaastra JS, Peterson JR, Paerels FBS, Mittaz JPD, et al. 2001. *Astron. Astrophys.* 365:L87–L92
204. Tozzi P, Norman C. 2001. *Ap. J.* 546:63–84
205. Tozzi P, Scharf C, Norman C. 2001. *Ap. J.* 542:106–119
206. Trümper J. 1993. *Science* 260:1769–1771
207. Valageas P., Silk J. 1999. *Astron. Astrophys.* 350:725–742
208. van Dokkum PG, Franx M. 2001 *Ap. J.* 553:90–102
209. van Haarlem MP, Frenk CS, White SDM. 1997. *MNRAS* 287:817–832
210. van Waerbeke L, Mellier Y, Radovich M, Bertin E, Dantel-Fort M, et al. 2001. *Astron. Astrophys.* 374:757–769
211. Venemans BP, Kurk JD, Miley GK, Röttgering HJA, van Breugel W, et al. 2002 *Ap. J.* 569:L11–L14
212. Viana PTP, Liddle AR. 1999. *MNRAS* 303:535–545
213. Viana PTP, Nichol RC, Liddle AR. 2002. *Ap. J.* 569:L75–L78
214. Vikhlinin A, McNamara BR, Forman W, Jones C. Hornstrup A, Quintana H, et al. 1998a. *Ap. J. Lett.* 498:L21–24
215. Vikhlinin A, McNamara BR, Forman W, Jones C, Quintana H, Hornstrup A. 1998b. *Ap. J.*, 502:558–581
216. Voit GM. 2000. *Ap. J.* 543:113–123
217. Voit GM, Bryan GL. 2002. *Nature* 414:425–427
218. White DA. 2000. *MNRAS* 312:663–688
219. White DA, Jones C, Forman W. 1997. *MNRAS* 292:419–467
220. White SDM, Efstathiou G, Frenk CS. 1993. *MNRAS*, 262: 1023–1028
221. White SDM, Navarro JF, Evrard AE, Frenk CS. 1993. *Nature* 366:429–433
222. Wu KKS, Fabian AC, Nulsen PEJ. 2000. *MNRAS* 318:889–912
223. Wu X-P, Xue Y-J, Fang L-Z. 1999. *Ap. J.* 524:22–30
224. Yamada M, Fujita Y. 2001. *Ap. J.* 553:145–148
225. Yee HKC, Ellingson E, Carlberg RG. 1996. *Ap. J. Suppl.* 102:269–287
226. York DG, Adelman J, Anderson JE Jr, Anderson SF, Annis J, et al. 2000. *Astron. J.* 120:1579–1587
227. Zheng W, Ford H, Tsvetanov Z, Davidsen A, Szalay A, et al. 2002. In *Lighthouses of the Universe*, in press
228. Zwicky F. 1937. *Ap. J.* 86:217–246
229. Zwicky F, Herzog E, Wild P. 1966. *Catalogue of galaxies and of clusters of galaxies*. Pasadena: California Institute of Technology

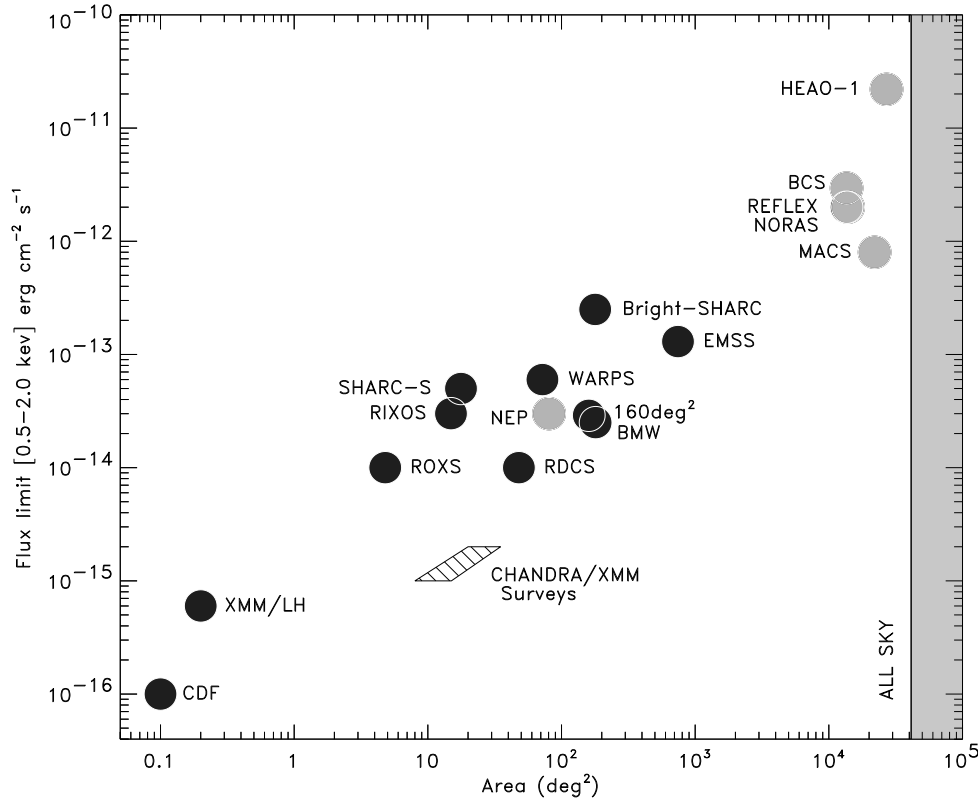


Figure 4: Solid angles and flux limits of X-ray cluster surveys carried out over the last two decades. References are given in the text. Dark filled circles represent serendipitous surveys constructed from a collection of pointed observations. Light shaded circles represent surveys covering contiguous areas. The hatched region is a predicted locus of future serendipitous surveys with *Chandra* and *Newton-XMM*.

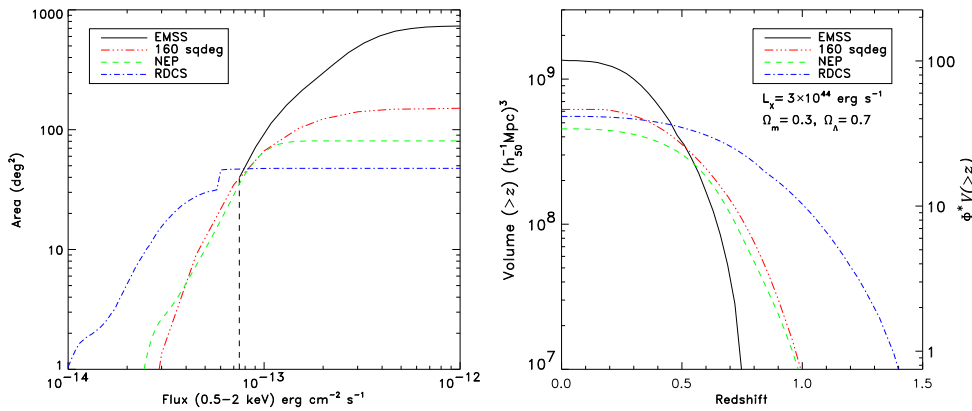


Figure 5: (*Left*) sky coverage as a function of X-ray flux of several serendipitous surveys; (*Right*) corresponding search volumes, $V(> z)$, for a cluster of given X-ray luminosity ($L_X = 3 \times 10^{44} \text{ erg s}^{-1} [0.5 - 2 \text{ keV}] \simeq L_X^*$). On the right axis the volume is normalized to the local space density of clusters, ϕ^* .

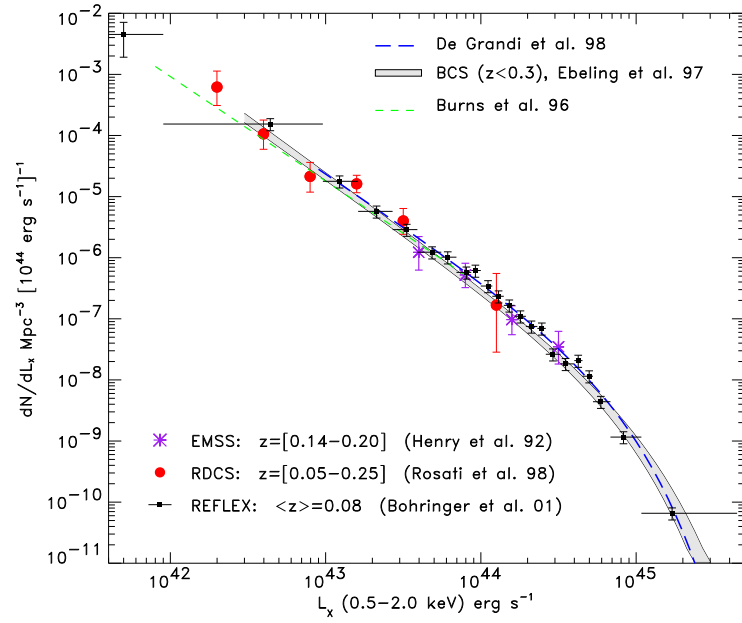


Figure 6: Determinations of the local X-ray Luminosity Function of clusters from different samples (an Einstein–de-Sitter universe with $H_0 = 50 \text{ km s}^{-1} \text{ Mpc}^{-1}$ is adopted). For some of these surveys only best fit curves to XLFs are shown.

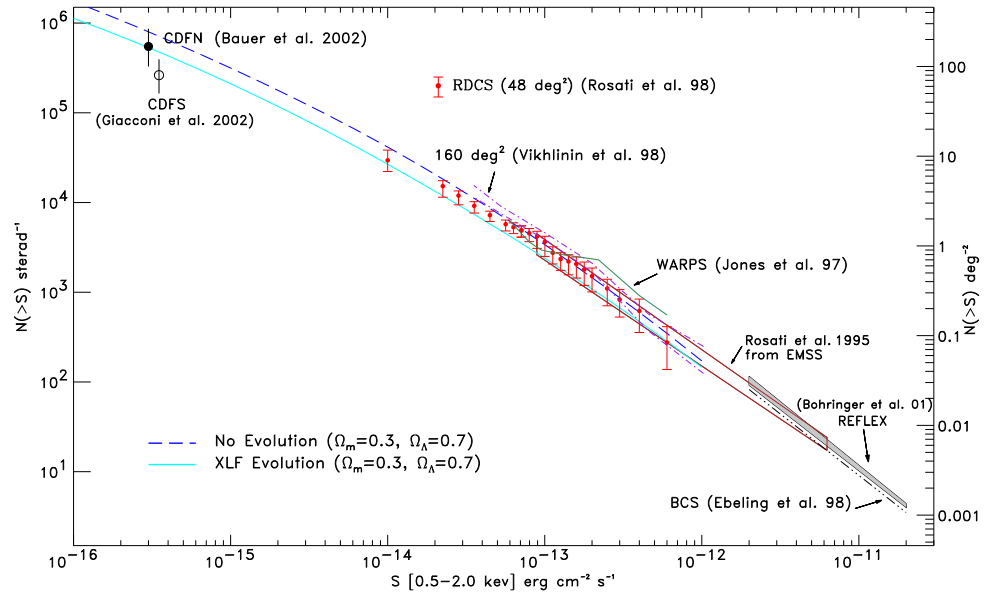


Figure 7: The cluster cumulative number counts as a function of X-ray flux ($\log N - \log S$) as measured from different surveys.

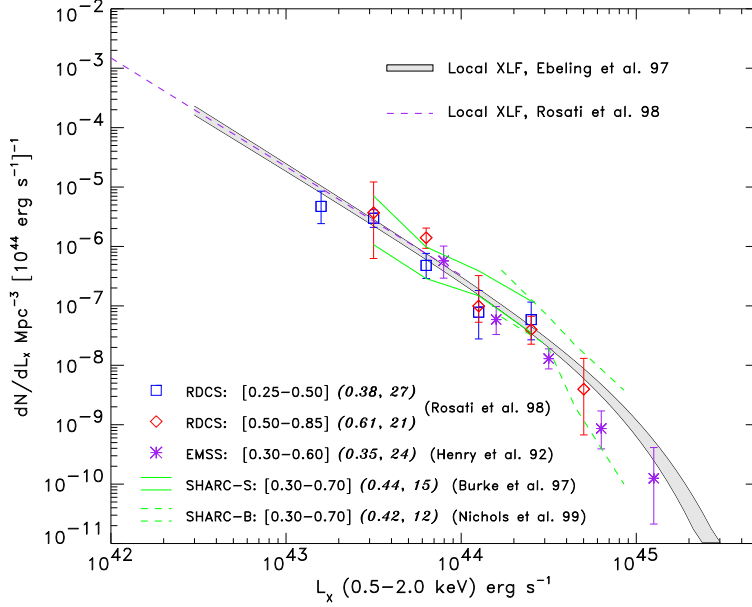


Figure 8: The X-ray Luminosity Function of distant clusters out to $z \simeq 0.8$ compiled from various sources and compared with local XLFs (an Einstein–de-Sitter universe with $H_0 = 50 \text{ km s}^{-1} \text{ Mpc}^{-1}$ is adopted). Numbers in parenthesis give the median redshift and number of clusters in each redshift bin.

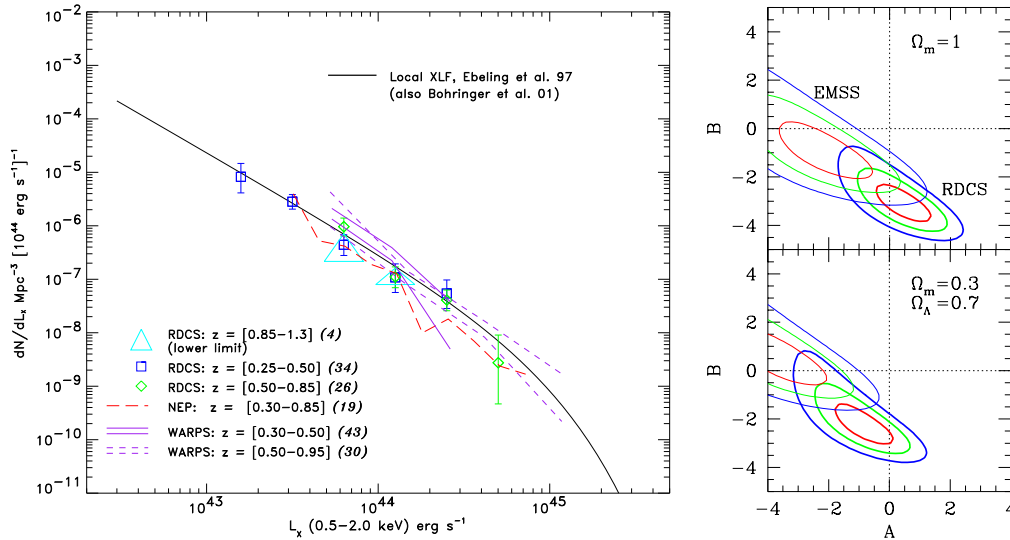


Figure 9: (*Left*) the latest compilation of distant XLFs (RDCS: Rosati et al. 2000; NEP: Gioia et al. 2001; WARPS: Jones et al. 2000; an Einstein–de-Sitter universe with $H_0 = 50 \text{ km s}^{-1} \text{ Mpc}^{-1}$ is adopted). Right panel: Maximum-likelihood contours (1, 2 and 3 σ confidence level) for the parameters A and B defining the XLF evolution for the RDCS and EMSS samples (for two different cosmologies): $\phi^* = \phi_0(1+z)^A$, $L^* = L_0^*(1+z)^B$ (see Equation 7).

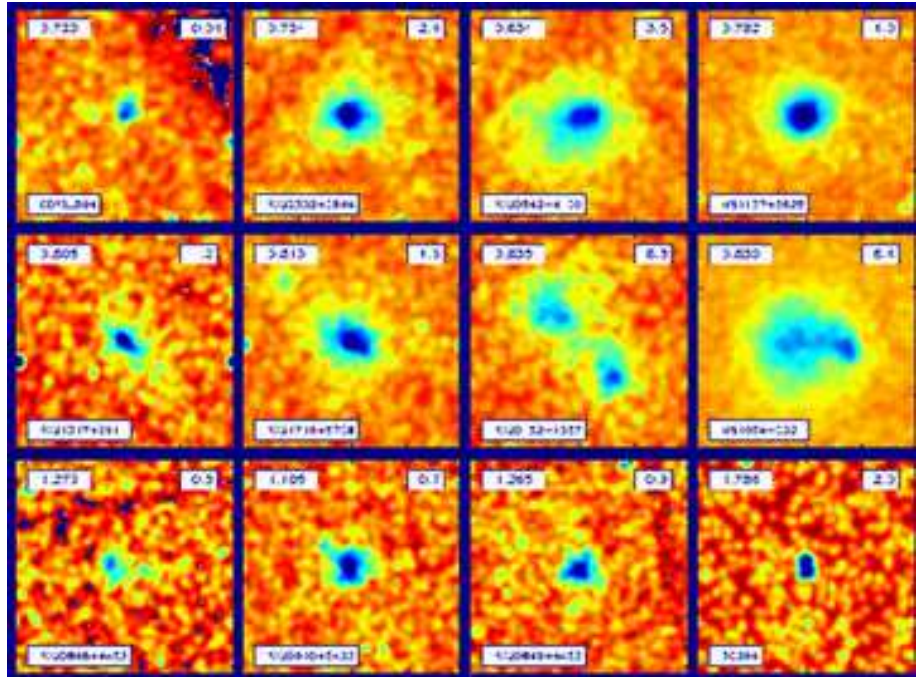


Figure 10: *Chandra* archival images of twelve distant clusters at $0.7 < z < 1.3$. Labels indicate redshifts (upper left) and X-ray luminosities (upper right) in the rest frame [0.5-2] keV band, in units of 10^{44} erg s^{-1} . All fields are 2 Mpc across; the X-ray emission has been smoothed at the same physical scale of 70 kpc ($h = 0.7, \Omega_m = 0.3, \Omega_\Lambda = 0.7$).

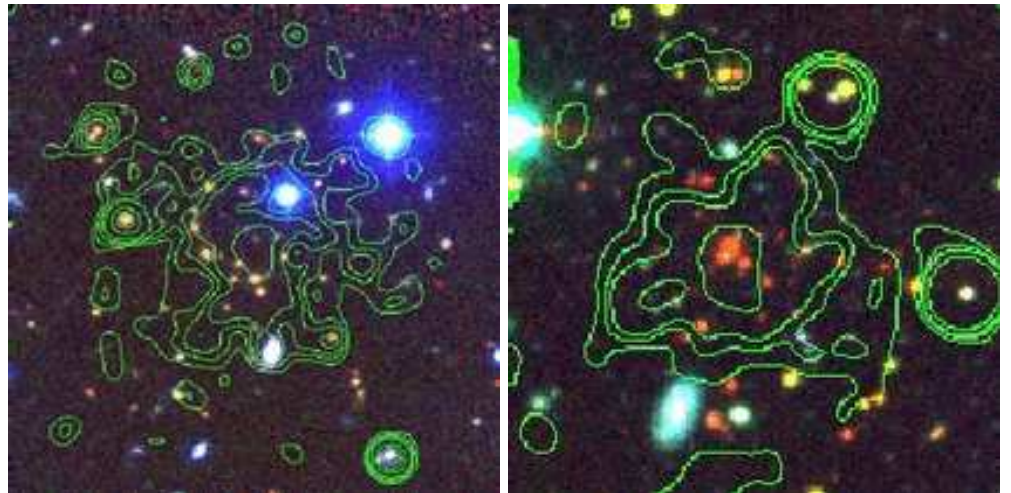


Figure 11: Color composite images combining optical and near-IR imaging of two X-ray selected clusters at $z > 1$. Overlaid contours map the X-ray emission detected by *Chandra/ACIS-I*. (*Left*) RXJ0910+5422 at $z = 1.11$ (Stanford et al. 2002); (*right*) RXJ0849+4452 at $z = 1.26$ (Rosati et al. 1999, Stanford et al. 2001). The two fields are 1.5 arcmin across ($\simeq 1h_{50}^{-1}$ Mpc at these redshifts).

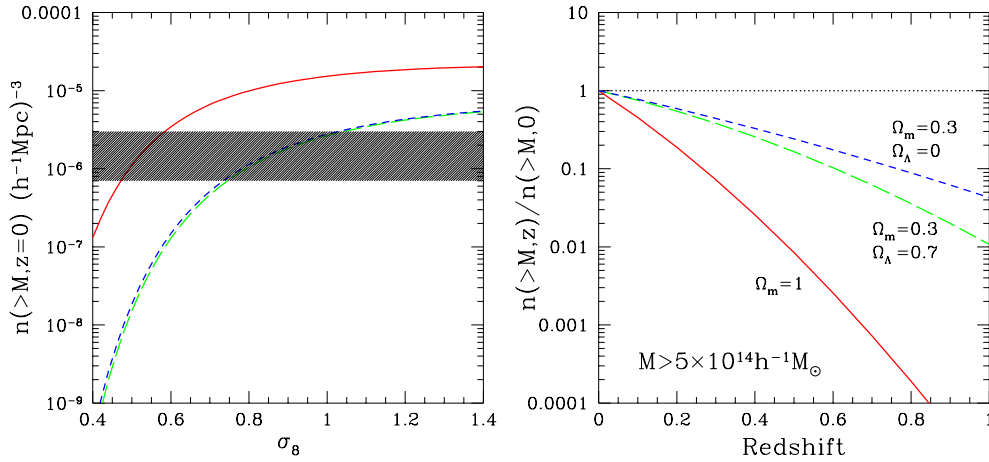


Figure 12: The sensitivity of the cluster mass function to cosmological models. (*Left*) The cumulative mass function at $z = 0$ for $M > 5 \times 10^{14} h^{-1} M_\odot$ for three cosmologies, as a function of σ_8 , with shape parameter $\Gamma = 0.2$; solid line: $\Omega_m = 1$; short-dashed line: $\Omega_m = 0.3, \Omega_\Lambda = 0.7$; long-dashed line: $\Omega_m = 0.3, \Omega_\Lambda = 0$. The shaded area indicates the observational uncertainty in the determination of the local cluster space density. (*Right*) Evolution of $n(>M, z)$ for the same cosmologies and the same mass-limit, with $\sigma_8 = 0.5$ for the $\Omega_m = 1$ case and $\sigma_8 = 0.8$ for the low-density models.

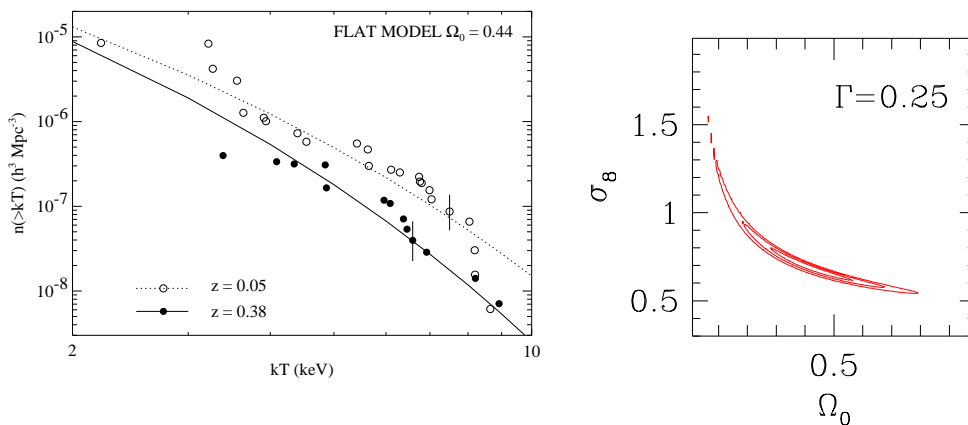


Figure 13: (*Left*) The cumulative X-ray temperature function for the nearby cluster sample by Henry & Arnaud (1991) and for a sample of moderately distant clusters (from Henry 2000). (*Right*) Probability contours in the $\sigma_8 - \Omega_m$ plane from the evolution of the X-ray temperature function (adapted from Eke et al. 1998).

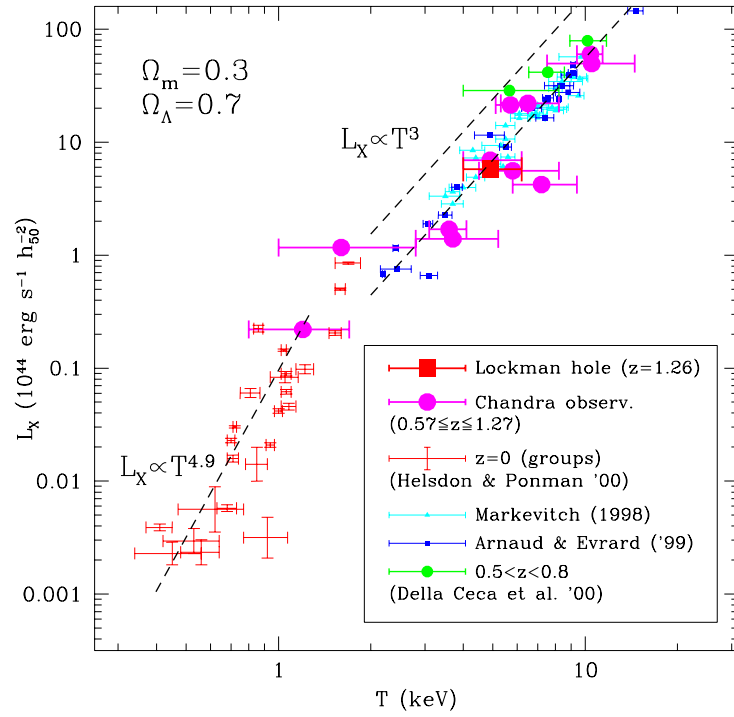


Figure 14: The (bolometric) luminosity–temperature relation for nearby and distant clusters and groups compiled from several sources (see Borgani et al. 2001b, Holden et al. 2002). The two dashed lines at $T > 2$ keV indicate the slope $\alpha = 3$, with normalization corresponding to the local L_X – T relation (lower line) and to the relation of Equation 14 computed at $z = 1$ for $A = 1$. The dashed line at $T < 1$ keV shows the best–fitting relation found for groups by Helsdon & Ponman (2000).

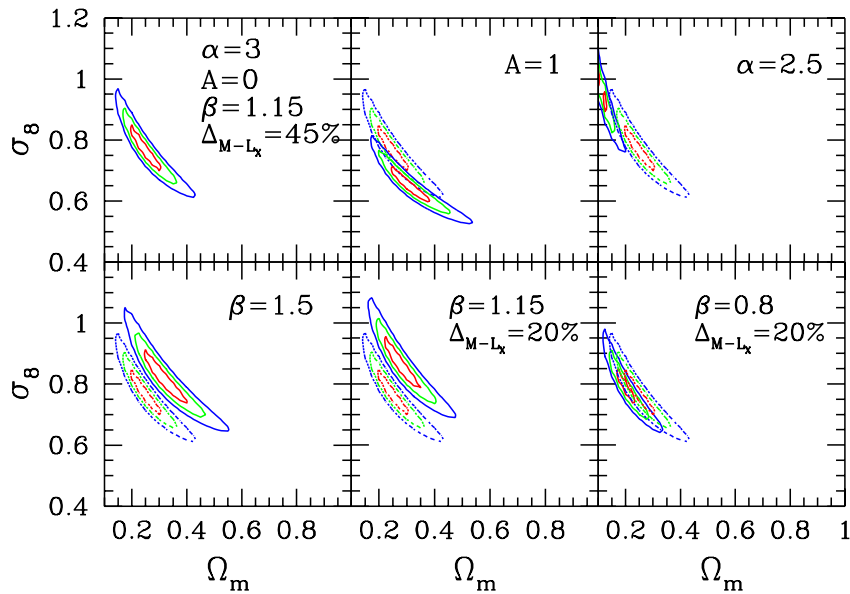


Figure 15: Probability contours in the σ_8 - Ω_m plane from the evolution of the X-ray luminosity distribution of RDCS clusters. The shape of the power spectrum is fixed to $\Gamma = 0.2$. Different panels refer to different ways of changing the relation between cluster virial mass, M , and X-ray luminosity, L_X , within theoretical and observational uncertainties (see also Borgani et al. 2001b). The upper left panel shows the analysis corresponding to the choice of a reference parameter set. In each panel, we indicate the parameters which are varied, with the dotted contours always showing the reference analysis.